An Insight into the Low-Temperature Thermal Evolution of the covered eastern Gawler Craton margin: the Stuart Shelf Basement

Thesis submitted in accordance with the requirements of the University of Adelaide for an Honours Degree in Geology/Geophysics

Christopher Wayne Trenouth

November 2015

THE UNIVERSITY of ADELAIDE

AN INSIGHT INTO THE LOW-TEMPERATURE THERMAL EVOLUTION OF THE COVERED EASTERN GAWLER CRATON MARGIN: THE STUART SHELF BASEMENT

ABSTRACT

Multi-method thermochronology applied to the eastern Gawler Craton, beneath the Stuart Shelf cover (Olympic Dam Domain, South Australia), reveal multiple episodes of exhumation. Modelled data from Apatite Fission Track (AFT) analysis identifies four time periods where the eastern Gawler Craton basement experienced cooling into AFT closure temperatures (~60-120°C); at1050 ± 55 Ma (Mesoproterozoic), 439 ± 14 Ma (late Ordovician-Silurian), 304 ±36 Ma (mid-Carboniferous-mid Permian) and 245 ± 52 Ma (late Permian-early Jurassic). In addition, the Carboniferous and Jurassic peaks are supported by zircon (ZHe) and apatite (AHe) (U-Th-Sm)/ He results. The Ordovician peak is interpreted as resulting from the final pulses of the Delamerian Orogeny partially, mixed with the first pulses of the Alice Springs Orogeny. The Carboniferous-Permian event is linked with widespread exhumation likely due to the final pulses of the Alice Springs Orogeny (~300Ma). The preserved Mesoproterozoic event presents new AFT data in the area and coincides with some recent studies. However, it occurs only in samples obtained from the Gawler Range Volcanics and more prominent in core depth shallower than 500m. The late Permian-early Jurassic event is comparable to events believed have to stemmed from hydrothermal events. This event compliments AFT studies in the northern Flinders Ranges. The Late Ordovician-Silurian and Carboniferous-early Permian AFT pulses confirm events seen in studies of surrounding regions. Other geochronological studies around the Olympic dam area indicate that this pulse, either results from a localised hydrothermal event or distal effects of the Musgravian Orogeny. The Jurassic event suggests that the hydrothermal effect on AFT ages may be more widespread event and not just localised to the northern Flinders Ranges as previously thought. The Ordovician event represents mixing between Delamerian and Alice Springs Orogenies. The Carboniferous-Permian event represents late distal effects of the Alice Springs Orogeny. These events match those of surrounding regions.

KEYWORDS

Exhumation, eastern Gawler Craton, Stuart Shelf, Olympic Dam Domain, Low-Temperature Thermochronology, Apatite Fission Track, Apatite Helium, Zircon Helium, South Australia

TABLE OF CONTENTS

LIST OF FIGURES AND TABLES

points have the same error bar indicated by the axis about the origin on the left showing ± 2σ. The closer an individual data point is to the age axis (right side), the more precise the measurement is, as seen by the horizontal precision axis directly below the plot (Boone *et al*., .2013). The colour assigned to each individual point indicates the uranium concentration in ppm of that particular grain, which corresponds to the colour scheme illustrated at the bottom of the figure. The units for the uranium scale are ppm. This plot was constructed using Radial plotter (Vermeesch *et al*., 2009).

Figure 8: Radial plots of single grain apatite fission track ages for samples pooled by depth and corresponding length distribution histograms for pooled sets. A) shallow samples (<500m) B) shows intermediate samples (500-800m) and C) shows pooled data for samples below 800mThe age for each point on the diagram is obtained by projecting a line from the origin onto the right curved axis in Ma. The central age for the sample is given at the top of the figure. A key feature of the radial plot is that all points have the same error bar indicated by the axis about the origin on the left showing ± 2σ. The closer an individual data point is to the age axis (right side), the more precise the measurement is, as seen by the horizontal precision axis directly below the plot (Boone *et al*., .2013). The colour assigned to each individual point indicates the uranium concentration in ppm of that particular grain, which corresponds to the colour scheme illustrated at the bottom of the figure. The units for the uranium scale are ppm. This plot was constructed using Radial plotter (Vermeesch *et al*., 2009).

Figure 9: Radial plots of single grain apatite fission track ages for all samples. AFT peaks are in purple, AHe peaks are in green and ZHe peaks are in blue. The age for each point on the diagram is obtained by projecting a line from the origin onto the right curved axis in Ma. The central age for the sample is given at the top of the figure. A key feature of the radial plot is that all points have the same error bar indicated by the axis about the origin on the left showing ± 2σ. The closer an individual data point is to the age axis (right side), the more precise the measurement is, as seen by the horizontal precision axis directly below the plot (Boone *et al*., .2013). The colour assigned to each individual point indicates the uranium concentration in ppm of that particular grain, which corresponds to the colour scheme illustrated at the bottom of the figure. The units for the uranium scale are ppm. This plot was constructed using Radial plotter (Vermeesch *et al*., 2009). The histogram shows the length distribution of measured confined tracks from all samples.

Figure 10: A TMI image indicating the gap is the regional low temperature exhumation of Australia (South Australia in particular) is seen in figure 10, which shows comparison between the central ages obtained by this study for the buried eastern Gawler Craton with all AFT central ages obtained by studies in the surrounding regions mentioned in this study.

Table 1; Sampled drill core names, number (DH#), sample location (Latitude/Longitude; Easting/Northings), Sample Depth, sampled unit and overlying unit. Sampled units in grey represent Hutchinson Granite, yellow = Hiltaba Suite Granites, light orange= Donnington Suite, light purple= Gawler Range Volcanics (GRV), olive green= Un-named granitic gneiss, kingfisher blue= Gabbro. Overlying stratigraphic unit are identified as follows light blue= Dolomitic Tapley Hill Formation, light grey = Unnamed GIS Unit, dark orange/red= Pandurra Formation (Adelaidean basement), dark purple= Apilla Tillite, bottle green= Gairdner Dyke Swarm.

INTRODUCTION

Previous studies on the Phanerozoic landscape evolution of Australia have mainly focussed on the Australian coastline (Hall Hons thesis 2014). Studies attempting to manufacture dynamic topographic models of the topographic evolution of inland Australia (particularly South Australia) are incomplete, due to gaps in low-temperature thermochronological data, such as Apatite Fission Track (AFT) data from inland Australian Regions (Hall Hons. Thesis, 2014; Czarnota *et al*. 2014). Previous Apatite Fission Track (AFT) low temperature thermochronological studies have been carried out in the regions surrounding the Stuart Shelf such as the northern Flinders Ranges (Foster *et al*., 1994; Mitchel *et al*., 2002; Weisheit *et al*., 2014), the central and northern Gawler Craton (Reddy Hons. thesis 2014); (Gleadow *et al*., 2002;), the Peake and Denison Ranges (Hall Hons. thesis 2014), the Officer Basin (Tingate and Duddy, 1996) and throughout the Adelaide Fold Belt (Gibson and Stüwe, 2000; Mitchell *et al*., 1998), (Hall *et al.,* 2014). Hall *et al* (2014) infers that a Carboniferous cooling phase observed in the Central Gawler Craton (Gleadow *et al*. 2002; Boone *et al*., 2002) and in the Flinders Ranges (Foster *et al*., 1994; Mitchel *et al*., 2002; Weisheit *et al*., 2014) and is thought to represent regional exhumation throughout South Australia as a distal response to the Alice Springs Orogeny.

The Stuart Shelf is a platform of undeformed Neoproterozoic to lower Cambrian sedimentary sequence of Adelaide Rift System equivalents that overly and define the eastern boundary of the Archaean to Mesoproterozoic crystalline basement of the Gawler Craton in South Australia (Hand *et al*., 2007). While the Stuart Shelf region including the underlying basement has been extensively studied from a mineral

exploration prospective, a low-temperature thermal history of the eastern Gawler Craton basement has yet to be definitively investigated. This thesis aims to uncover the low temperature thermal history of the eastern Gawler Craton below the Stuart Shelf platform by applying multi-method thermochronology (apatite fission track (AFT) dating, zircon (U-Th-Sm)/He dating and apatite (U-Th-Sm)/He dating to discover whether the buried eastern margin of the Gawler Craton experiences a similar low temperature thermal history as observed for the surrounding regions outlined above. Apatite Fission Track (AFT) low temperature thermochronological studies have been carried out in the regions surrounding the Stuart Shelf such as the northern Flinders Ranges (Foster *et al*., 1994; Mitchel *et al*., 2002; Weisheit *et al*., 2014), the central and northern Gawler Craton (Reddy Hons. thesis 2014); (Gleadow *et al*., 2002), the Peake and Denison Ranges (Hall Hons. thesis 2014), the Officer Basin (Tingate and Duddy, 1996) and throughout the Adelaide Fold Belt (Gibson and Stüwe, 2000; Mitchell *et al*., 1998). A Carboniferous cooling phase has been observed in the Central Gawler Craton (Gleadow *et al*., 2002) and in the Flinders Ranges (Foster *et al*., 1994; Mitchel *et al*., 2002; Weisheit *et al*., 2014) and is thought to represent regional exhumation throughout South Australia as a distal response to the Alice Springs Orogeny. In addition for parts of the Flinders Ranges Ordovician cooling following the Delamerian Orogeny; ~480 and 440 Ma has been observed (Weisheit *et al*., 2014). Furthermore, studies in the Adelaide Fold Belt. Flinders Ranges and Gawler Craton have reported several more localised younger Mesozoic- Tertiary AFT ages (Mitchell *et al*., 1998; Gibson and Stüwe 2000) which are represent the effect of late Triassic –early Jurassic hydrothermal activity in the Flinders (Weisheit *et al*., 2014) and Cretaceous exhumation across Southern Australia (MacDonald *et al*., 2013).

This thesis presents low-temperature data from granitic, igneous and metamorphic samples from sections of drill cores below the Stuart Shelf platform along a roughly north-south trending profile to evaluate the thermal history along the whole length of the Stuart Shelf. The resulting data was then modelled providing a reconstruction of the study area from the Mesoproterozoic through to the Mesozoic. The results from this thesis shall be collaborated into a PhD thesis aiming to reconstruct the low temperature thermal history of South Australia on a regional scale.

BACKGROUND

The Stuart Shelf is a Proterozoic to lower Cambrian (Waterhouse *et al*., 2002) geological province representing a thin platform of Neoproterozoic and Palaeozoic aged sediments that cover crystalline Archaean-Mesoproterozoic aged rocks at the eastern border of the Gawler Craton (Parker *et al*., 1993) (figure 1).The Stuart Shelf is not a tectonic unit of the Gawler Craton. However, it defines the region of Neoproterozoic to Cambrian platformal sedimentation developed upon the existing Craton (Drexel et al., 1993). Its boundary is defined by the extent of the Pandurra Formation over the east-central Gawler Craton. The Pandurra Formation was deposited in the Cariewerloo Basin, a tectonic subdomain of the Gawler Craton (Drexel *et al*., 1993) The sedimentary rock sequence of the Stuart Shelf overlies the Pandurra Formation at the base, which mainly consists of sandstones, and ends with mostly reworked undifferentiated sedimentary layers deposited on a stable cratonic platform overlying the eastern margin of the Gawler Craton. Despite its location adjacent to the tectonically active Adelaide Geosyncline the Stuart Shelf has remained mostly undeformed since deposition (Preiss *et al*., 1987). The folded rocks of the Adelaide Geosyncline are separated from the undeformed Stuart Shelf by the Torrens Hinge Zone. The Tent Hill formation comprising the Cornaberra Sandstone and Arcoona Quartzite members of the Adelaidean Period, all inclusive of the Marinoan unit, Palaeozoic platform carbonates that make up the Arrowie Basin (including the Andamooka Limestone) that lap onto the Stuart Shelf from across the Torrens Hinge Zone, make up the shallowest sedimentary rocks on the Stuart Shelf. The Stuart shelf sequence unconformably overlies older sedimentary rocks of the Pandurra formation, which generally shows more structural features than the overlying Stuart Shelf, presumably due to tectonic activity that

predates the stable depositional conditions during and after Stuart Shelf deposition.

Drexel et al (1993) refers to this sequence as the Cariewerloo Basin.

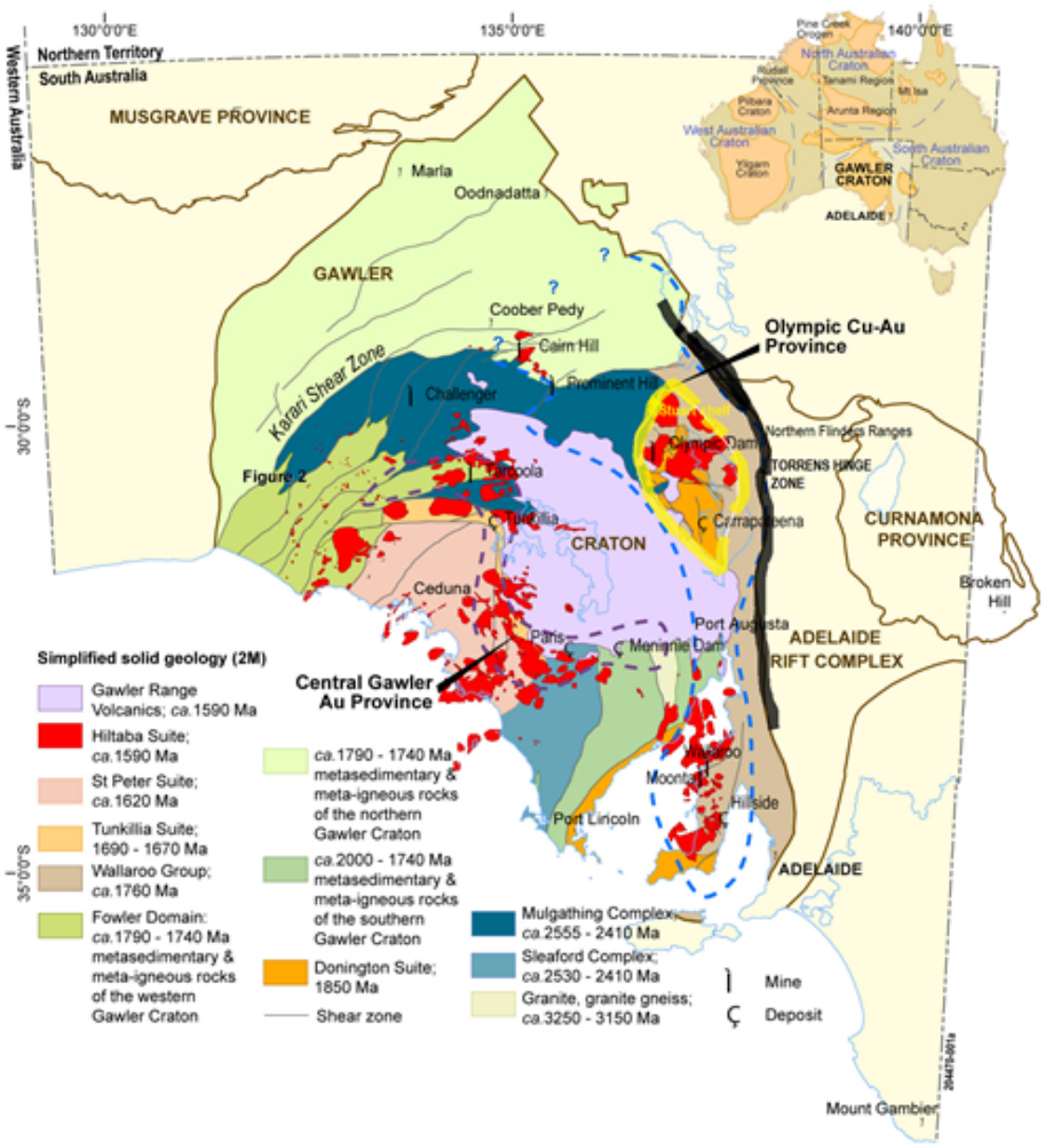

Figure 1: Interpreted solid geology of the Gawler Craton along with major Precambrian tectonic elements of South Australia. The location of the Olympic Cu-Au province and Olympic Dam are indicated. The Stuart Shelf is outlined in yellow and the Torrens Hinge Zone is represented by the thick black line (adapted from Jagodzinski *et al.*, 2015)

The northwest-southeast oriented strike of the Torrens Hinge Zone runs parallel to the western shore of Lake Torrens between Olympic Dam and Lake Eyre. It continues past the Peake- Denison Inliers to the north of the study area. The Torrens Hinge Zone represents a poorly understood deep crustal fracture zone that was very active during the Neoproterozoic and the Delamerian Orogeny. It was initiated during early Neoproterozoic extension and crosscuts older Proterozoic terrain boundaries (Teasdale *et al*., 2001)

The Stuart Shelf equivalents in the Adelaide Geosyncline are surrounded, and in some cases overlain, by three important sedimentary basins. The Late Carboniferous - Early Permian Arckaringa Basin comprises a mixture of sandstones, siltstones, diamictites and carbonaceous formations. The Eromanga Basin of Mesozoic age is composed of the Algebuckina Formation, Canda-owie Formation, and the Bulldog Shale, which only exist as remnants in the near vicinity of the Peake and Denison Inliers. The Torrens Basin of Cenozoic age (Preiss *et al*., 2002) to the east of the Torrens Fault is a large synclinal structure of folded Adelaide Geosyncline rocks that are infilled with Tertiary sediments to a depth of approximately 300m.

The Gawler Craton underwent widespread exhumation in the Cretaceous as seen in AFT data (Kohn *et al*., 2002; MacDonald *et al*., 2013). (Dyksterhuis and Müller 2008) claimed the rifting of Australia from and Antarctica and the closing of the Neo-Tethys Ocean was directly responsible for this Gawler Craton exhumation. We can assume that as the Stuart shelf lies on top of the Gawler Craton we should see similar AFT data.

AFT data obtained by Radke *et al* (1973) indicated an exhumation event in the Permian (266 ± 23 Ma). But because this study was taken from only one sample, we cannot rely on this, however other studies support this age. The cause of the AFT ages in the study above may be related to the after effects of the Alice Springs Orogeny that ended just before the Permian or possibly even the New England Orogeny. It could also be a result of the erosion of Carboniferous mountain belts that caused the Permian glacial event in the northern Gawler Craton. Regional uplift in the Cooper Basin, close to the Stuart Shelf, is suggested by the occurrence of major unconformities dated around 250 Ma (Reynolds *et al*., 2006) and this could be related to the ages in the study by Radke (1973). Very poorly constrained data in the Northern Flinders Ranges is also suggested to be related to this tectonic event.

METHODOLOGY

Samples were obtained following a NS transect, taken from the granitic basement of the eastern Gawler Craton below the Pandurra unconformity underneath the Stuart Shelf platform. The majority of the northern samples are located around Olympic Dam and the southern most of the samples were taken near Carrapateena and Punt Hill shown in figure 2 Samples BRD 1, Blanche 1, SAE 6, and samples from drill hole (DH); 1831650, 1831646, were all sourced from the Mesoproterozoic Hiltaba Suite Granite; samples PSC 7 SASC 3, SAE 11, GHDD 1, and two samples from DH RED 2, 2131363 and 2131364 were taken from the Mesoproterozoic Gawler Range Volcanics. Sample SHD 1 was taken from the Gneissic, Hutchinson group of Paleoproterozoic age, sample AS10D04 was taken from the Paleoproterozoic Dennington Granite Suite, sample NHD 1 was taken from unnamed gneissic granite with of Mesoproterozoic age and sample ASD 1 was taken from a fine grained gabbro of unknown age. Sample locations, coordinates and lithological description is shown in table 1 and locations are shown in

figure 2

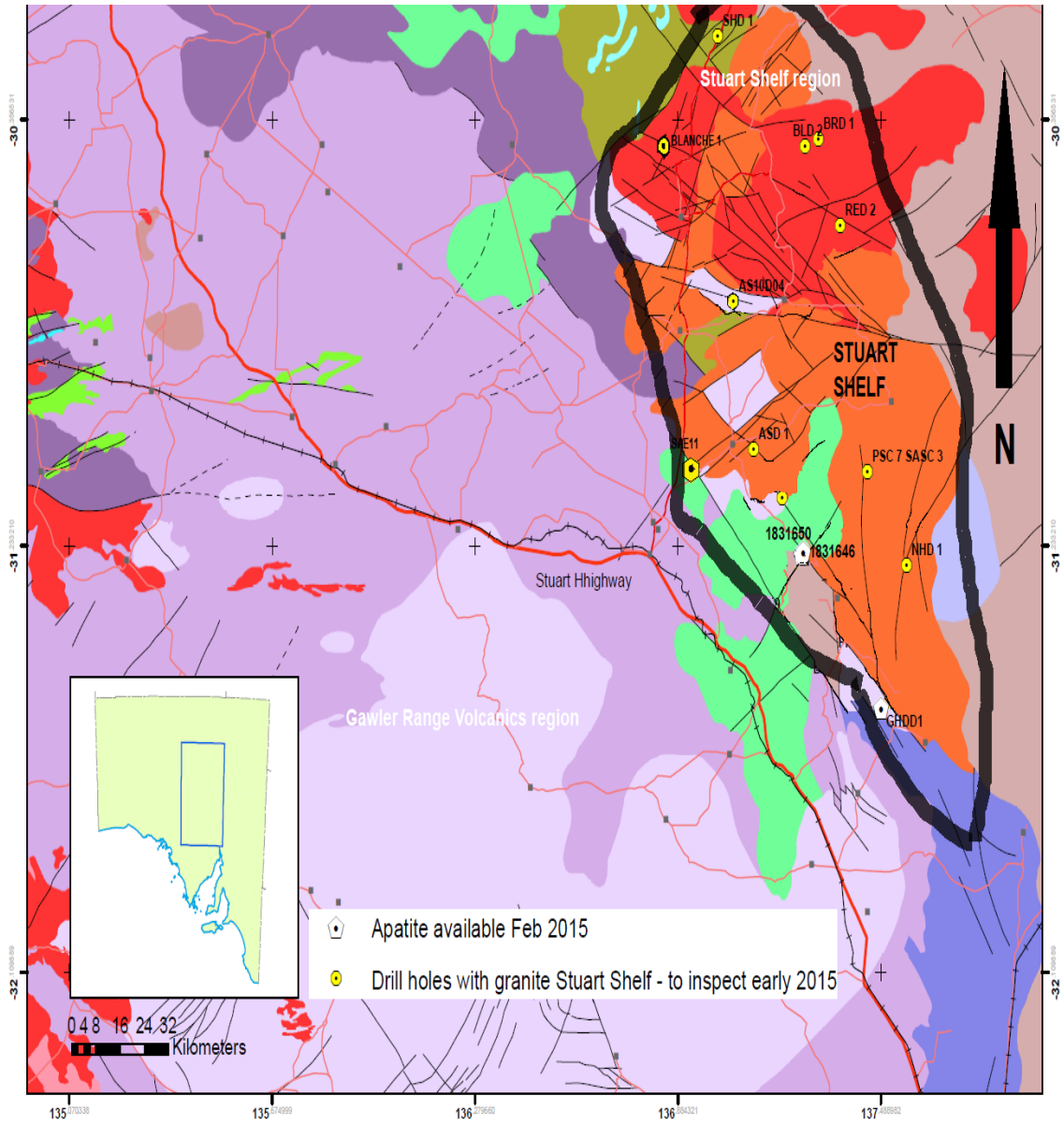

Figure 2: Basement map of the study region showing the study area outlined in black and the locations of sample locations with relation to underlying basement geology

Table 1; Sampled drill core names, number (DH#), sample location (Latitude/Longitude; Easting/Northings), Sample Depth, sampled unit and overlying unit. Sampled units in grey represent Hutchinson Granite, yellow = Hiltaba Suite Granites, light orange= Donnington Suite, light purple= Gawler Range Volcanics (GRV), olive green= Un-named granitic gneiss, kingfisher blue= Gabbro. Overlying stratigraphic unit are identified as follows light blue= Dolomitic Tapley Hill Formation, light grey = Unnamed GIS Unit, dark orange/red= Pandurra Formation (Adelaidean basement), dark purple= Apilla Tillite, bottle green= Gairdner Dyke Swarm.

DH name	DH #	Longitude	Latitude	Easting	Northing	Sample Depth	Sampled Unit	Overlying Unit
SHD 1	20828	137.002091	-30.185769	692755	6658935	857.5 - 858.4m	Hutchison Group	Tapley Hill Formation
BRD 1	170020	137.301673	-30.398105	721128	6634851	816- 817m	Hiltaba Suite	Dolomitic Tapley Hill Formation
AS10D04	259027	137.049772	-30.731497	696250	6598360	655.658.8m	Doington Suite	Tapley Hill Formation
RED 2	2131364	137.367642	-30.575543	727055	6615049	445-446m	Gawler Range Volcanics	Unnamed GIS Unit
RED 2	2131363	137.367642	-30.575543	727055	6615049	334-335.1m	Gawler Range Volcanics	Unnamed GIS Unit
PSC 7 SASC 3	139595	137.447937	-31.081659	733528	6558771	668.1-689.1m	Gawler Range Volcanics	Pandurra Formation
NHD 1	25369	137.565152	-31.274311	744219	6537157	535-536	Granitic gneiss (undefined unit)	Appila Tillite
SAE 6	165609	137.149384	-31.110437	704978	6556171	847.7-849.3m	Hiltaba Suite	Pandurra Formation
ASD 1	20722	137.108857	-31.03649	701269	6564443	961.5-962.4m	Fine-medium grained gabbro	Pandurra Formation
SAE 11	165125	136.937901	-31.073198	684878	6560671	1000.1-1001.1m	Gawler Range Volcanics	Pandurra Formation
BLANCHE 1	206086	36.7970873	-30.470106	672516	6627749	1000-1001m	Hiltaba Suite	Pandurra Formation
GHDD_1	253551	137.489862	-31.566319	736315	6504944	967.7-968.7m	Gawler Range Volcanics	Pandurra Formation
1831646	229979	137.252149	-31.251144	714464	6540377	667.05-667.3m	Hiltaba Suite	Pandurra Formation
1831650	229979	137.252149	-31.251144	714464	6540377	738.1-738.8m	Hiltaba Suite	Gairdner Dolerite/ Dyke Swarm

Apatite Fission Track Analysis

Apatite Fission Track (AFT) analysis is used to constrain the thermal history of a rock through the so-called Partial Annealing Zone (PAZ) between ~60-120°C (Gleadow *et al*., 2002; Wagner and Van Den Haute., 1992). AFT dating is based on the spontaneous fission decay of 238U that produces damage tracks (called fission tracks) within the mineral crystal lattice structure (Wagner and Van den Haute., 1992). These fission tracks are not retained in the crystal lattice at elevated temperatures (>120C) and only partially retained at PAZ temperatures (~60- 120C). Quantifying the radiation damage by fission track counting and measuring the associated 238U concentration can therefore be used to date when the rocks were cooled to subsurface temperatures. In addition, cooling and potential reheating rates can be estimated and modelled to reconstruct the subsurface thermal history of the study area.

After selection of appropriate sections of drill cores, samples underwent rock crushing and conventional mineral separation processes. Several samples (1831650, 1831646, 1831656, GHDD 1) were supplied as separates by Dr. Anthony Reid (Department of State Development). Apatites were then hand-picked individually, under a microscope, according to conventional selection criteria. Selected apatites were arranged in a raster, then mounted in epoxy resin, ground and polished to expose internal sections. Polished mounts then underwent chemical etching for 20 seconds in a 5M HNO3 solution at a temperature of 20°C to reveal the fission tracks.

The density of fission tracks in individual grains was determined by counting the number of fission tracks in a reference grid using an Olympus BX-51 microscope. Confined fission track lengths were measured were present, along with Dpar measurements and angles with respect to c-axis, which would later act as an aid to determine the rate of sample cooling through the apatite partial annealing zone (PAZ). Uranium concentration for each grain was determined using a Laser-Ablation Inductively-Coupled-Plasma Mass Spectrometer (LA-ICP-M) at Adelaide Microscopy (New Wave UP213 laser system coupled with an Argillent 7500 quadruple mass spectrometer), following analytical methods as outlined by De Grave *et al* (2012). Calibration of the LA ICP MS was carried out against a suite of NIST glass standards (NIST 610, NIST 612, NIST 614) of known uranium concentration (Pearce *et al*., 1997) and using Durango apatite and an in-house standard from Arkaroola as a secondary standard, while Ca 44 was used as an internal standard.

Two sessions were required to analyse all selected grains. LA ICP MS data was processed off-line via an in-house Excel spreadsheet. An AFT central age of 33.4 ± 1.9 Ma was obtained for the Durango Apatite standard throughout this study as shown in figure 2, which is within the error range obtained for the published Durango Apatite AFT age ; 31.44± 0.18 Ma (McDowell *et al*.,2005). Strongly zoned grains gave unreliable Uranium concentration and were therefore excluded from further AFT age calculations.

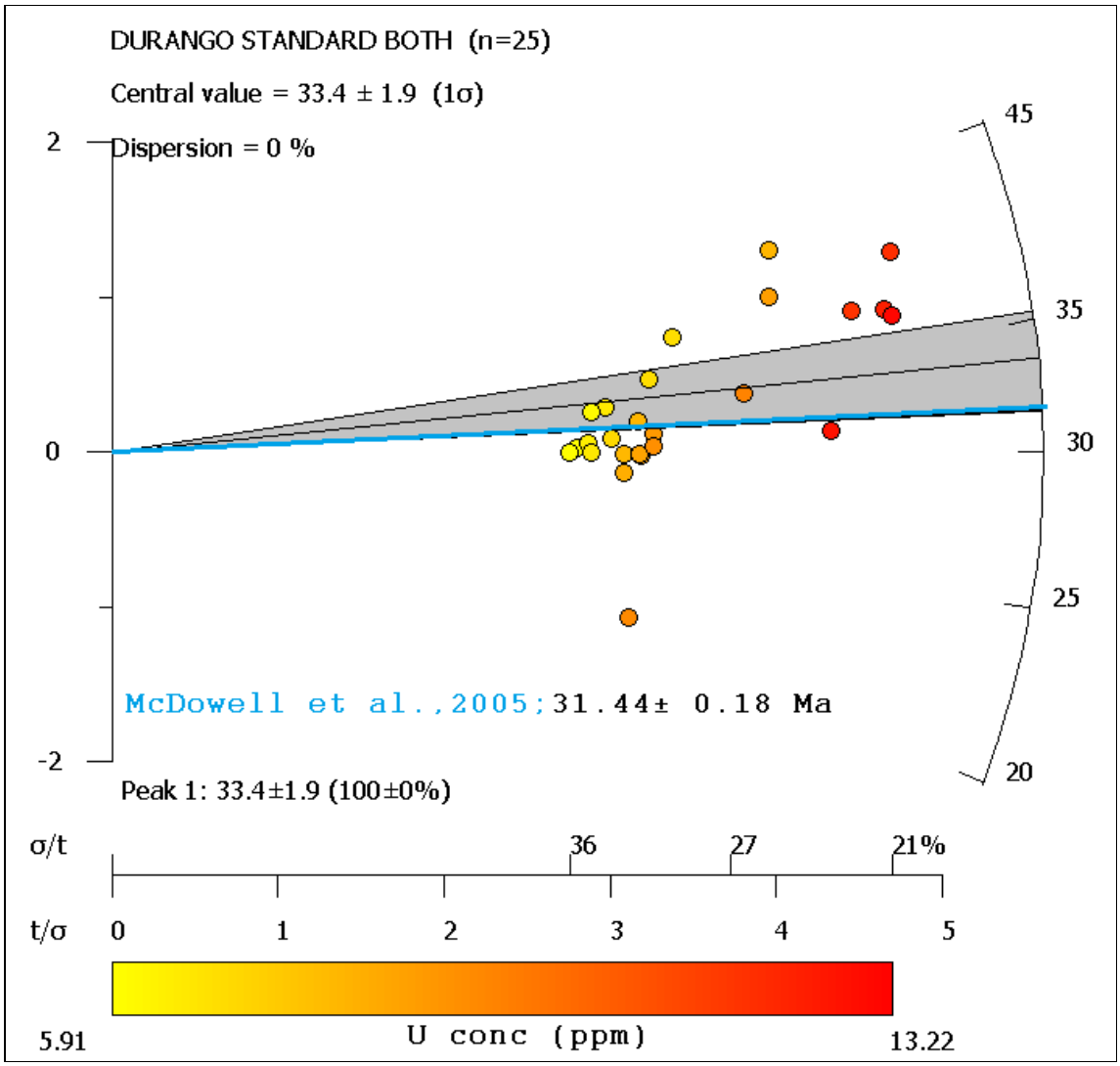

Figure 3: Radial plot of measured Durango (Grey 33.4±1.9Ma) age obtained in study compared to Durango standard age (31.44±0.18Ma) from McDowell *et al.*, 2005. The age for each point on the diagram is obtained by projecting a line from the origin onto the right curved axis in Ma. The central age for the sample is given at the top of the figure. A key feature of the radial plot is that all points have the same error bar indicated by the axis about the origin on the left showing ± 2σ. The closer an individual data point is to the age axis (right side), the more precise the measurement is, as seen by the horizontal precision axis directly below the plot (Boone *et al.*, .2013). The colour assigned to each individual point indicates the uranium concentration in ppm of that particular grain, which corresponds to the colour scheme illustrated at the bottom of the figure. The units for the uranium scale are ppm. This plot was constructed using Radial plotter (Vermeesch *et al.*, 2009).

Apatite (U-Th-Sm)/ He (Ahe) and Zircon (U-Th-Sm)/ He (Zhe) Dating

Apatite (U-Th-Sm)/ He (AHe) and zircon (U-Th-Sm)/ He (ZHe) analysis was carried out to compliment the AFT data as well as to refine subsequent thermal history modelling to temperatures between ~75-45°C and ~200- 170°C for AHe and ZHe (Farley *et al*., 2002; Reiners *et al*., 2004). Twenty grains from four zircon, and one apatite separate were selected based on grain quality to be sent to the John De Laeter Centre at Curtin University. Grains were picked individually and loaded into Pt (apatite) and Nb tubes at ~960°C and ~1250°C for apatite and zircon grains respectively. Measurement of the resulting He4 concentration was carried out using a Pfeiffer Prisma QMS-200 mass spectrometer, following this the samples were digested in acid and measurement of U, Th and Sm concentration was taken using an Agilent 7500S mass spectrometer. Detailed methodology for apatite and zircon (U-Th-Sm)/ He analysis is given by Danišík *et al* (2012).

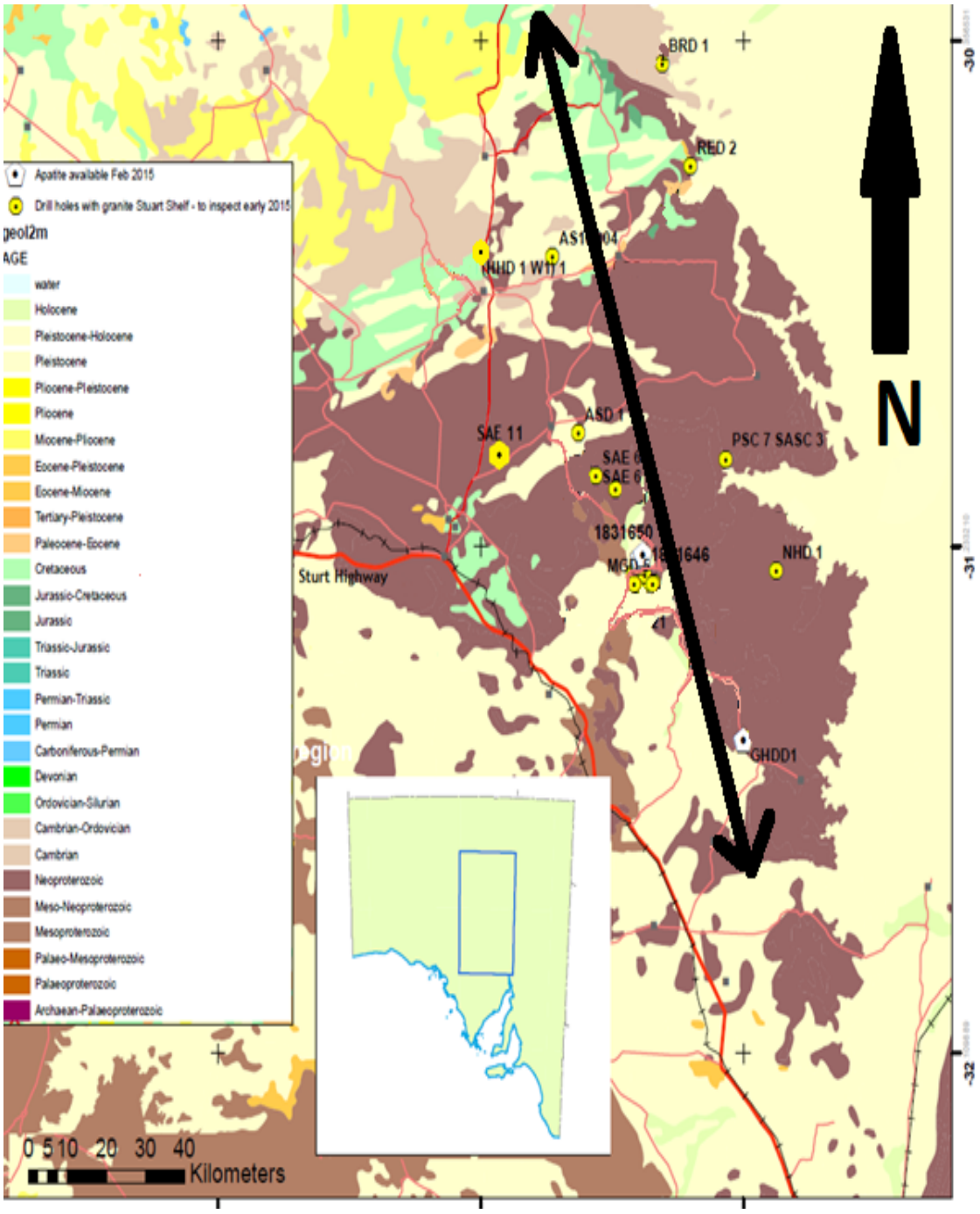

Figure 4:; a 2M geological map of the study area showing the location of samples included in this study and the geologic age of the surface geology

Radial plots and thermal history modelling

AFT central ages were calculated using Radial Plotter 7.4 (Vermeesch, 2009). For samples with age dispersion greater than 20%, multiple age components were identified using the automatic mixture model in the Radial Plotter Software. The automatic mixture model in Radial Plotter 7.4 carried out the un-mixing process, with U concentration (ppm) used as a visual guide to validate the resulting modelled age-components based on lattice damage.

RESULTS

Thermochronometric analysis was carried out on 10 sample locations along a roughly north/south trend covering the Stuart Shelf region Figure 3) .The results are given in order of decreasing sample depths within the sampled drill cores.

Sample SHD1 is the most northward located sample in the study region and was taken from a depth of 857.5- 858.4m. For this sample, 27 apatites were analysed, returning a central AFT age of 328 ± 17 Ma (figure 5a). Given the rather large (~24%) dispersion in single grain data, the AFT age population was decomposed into three peaks using the automatic mixer algorithm in Radial plotter (Vermeesch *et al.* 2009).The oldest AFT peak (based on 30% of the data) was constrained to 448 ± 24 Ma (late Ordovician-early Silurian). Furthermore an intermediate Carboniferous AFT age peak of 321 ± 27 Ma (based on 38% of the data) and youngest (based on 32% of the data) returned a 248 ± 16 Ma (late Triassic) AFT age peak was obtained. Sixty eight confined fission track lengths were measured, exhibiting a slightly bimodal distribution with data slightly skewed to the left. The average track length obtained was 11.74µm with a standard deviation of 1.80µm, which indicates a prolonged residence in the apatite fission track partial annealing zone.

Sample SAE11 was obtained from a depth of 1000.1- 1001.1m and located closer to the centre of the study region. For this sample, only 10 apatites could be analysed with a central AFT age of 526 ± 68 Ma (figure 5b). Given the rather large (~34%) dispersion in single grain data, the AFT age population was decomposed into two peaks using the automatic mixer algorithm in Radial plotter (Vermeesch *et al.,* 2009). The oldest peak (comprising two single grain ages) was constrained to ~1057 Ma in the

Mesoproterozoic, the youngest (based on 80 ± 13% of the data) returned a 434 ± 35 Ma (Silurian) AFT age peak. The measured confined track length distribution for this sample is skewed to the left with a mean AFT length of 10.38µm and a standard deviation of 2.13µm, indicating a protracted PAZ signature.

Sample ASD1 was obtained from a depth of 961.5 - 962.4m and located near the centre of the study region. For this sample, only 4 apatites could be analysed with a central AFT age of 429 ± 21 Ma (Silurian) (figure 5c). Given the low number of analysed apatite grains and associated small age dispersion, the data was not further decomposed (Vermeesch *et al.,* 2009). With length measurements unable to be recovered for this sample, the cooling history is poorly constrained.

Sample Blanche 1 was obtained from a depth of 1000-1001m and located in close proximity to the Olympic Dam site. For this sample, only 2 apatites could be analysed with a central AFT age of 345 ± 41Ma (early Carboniferous) (figure 5d), which could not be further decomposed in age-peaks. Given the rather small dispersion (8.9%) in single grain data, the AFT age population was decomposed into a single peak using the automatic mixer algorithm in Radial plotter (Vermeesch *et al.,* 2009). Zircon (U-Th-Sm)/He analysis was conducted on 4 zircon grains for this sample, constraining a mean late Permian- early Triassic ZHe age of 250 ± 15Ma (based on 3 single grain ages. One additional zircon grain gave a Cretaceous ZHe signal (132.5 ± 9.2 Ma). The number of reliable fission track length data was insufficient to comment on the AFT cooling rate for this sample.

Sample NHD1 was obtained from a depth of 535.5 -536m at the easternmost location in the study area. For this sample, only 6 apatites could be analysed with a central AFT age of 383 ± 48 Ma (figure 6a). Given the rather large dispersion (21%) in single grain data, the AFT age population was decomposed into two peaks using the automatic mixer algorithm in Radial plotter (Vermeesch *et al.,* 2009). The oldest peak (comprising 5 single grain ages) was constrained to a 426 ± 42 Ma (Silurian) AFT age peak, the youngest (based on a single grain) returned a single 190 ± 50 Ma (early Jurassic) AFT age. The number of reliable fission track length data was insufficient to comment on the AFT cooling rate for this sample.

Sample PSC 7 SASC 3 was obtained from a depth of 688.1-689.1m and was taken north of sample NHD 1 in the centre of the study area. For this sample, only 5 apatites could be analysed with a central AFT age of 383 ± 39 Ma (figure 6b). Twenty seven confined fission track length measurements exhibited a slightly bimodal distribution with data slightly skewed to the left. The average track length obtained was 10.52µm with a standard deviation of 1.76µm, which indicates a prolonged residence in the apatite fission track partial annealing zone.

Sample AS10D04 was obtained from a depth of 655.5 -658.8 and located in the north of the study area. For this sample, only 2 apatites could be analysed (figure 6c), returning a central AFT age of 371 ± 34 Ma, which could not be further decomposed in age-peaks (figure 6b). Zircon (U-Th-Sm)/ He analysis of 5 zircon grains for this sample constrained two age populations of 291.0 ± 6.9 Ma (late Carboniferous- early Permian age) comprising 3 single grain ages and 169.6 Ma (Jurassic) based on 2 grains'

Samples 1831646 and 1831650 were obtained from drill-hole MGD 45 at depths of 667-667.3m and 738.1-738.8m respectively and located near to the centre of the study region. For these samples, 48 apatites were analysed with a pooled central AFT age of 359 ± 13 Ma (figure 6d). Given the rather large (~18%) dispersion in single grain data, the AFT age population was decomposed into two peaks using the automatic mixer algorithm in Radial plotter (Vermeesch *et al.,* 2009). The oldest peak (comprising 47% of single grain ages) was constrained to 438 ± 20 Ma in the Silurian, the youngest (based on 53% of the data) returned a 298±14Ma (late Carboniferous-early Permian) AFT age peak. Zircon (U-Th-Sm)/ He analysis of 5 zircon grains from sample 1831650 constrained two age populations of 181.3 ± 6.6 Ma (late Jurassic) comprising 2 single grain ages and 74.7 ± 2.9 Ma (late Cretaceous) based on 3 grains. A combined total of 119 confined fission track length measurements exhibited a unimodal distribution with data slightly skewed to the right. The average track length obtained was 10.39µm with a standard deviation of 1.96µm, which indicate a prolonged residence in the apatite fission track partial annealing zone.

Samples 2131363 and 2131364 were obtained from drill-hole RED 2 located in the north of the study area, at depths of 334.1- 335.1m and 445 -446m. For these samples, 20 apatites were analysed with a central AFT age of 629 ± 71 Ma (figure 7). Given the rather large (46%) dispersion in single grain data, the AFT age population was decomposed into two peaks using the automatic mixer algorithm in Radial plotter (Vermeesch *et al.,* 2009). The oldest peak (comprising 45% of single grain ages) was constrained to a Mesoproterozoic (1047 ± 59 Ma) age peak, the youngest (based on 55% of the data) returned a 425 ±25 Ma (Silurian) AFT age peak. Apatite (U-Th-Sm)/

He analysis of two apatite grains from sample 2131364 returned two age populations of 257.1 ± 21 Ma (early Triassic) and the youngest 211.9 ± 43.5 Ma (late Triassic). A total of 28 confined fission track length measurements were obtained for sample 2131363 only, exhibiting a bimodal distribution with data slightly skewed to the right. The average track length obtained was 10.03µm with a standard deviation of 2.14µm, which indicate a prolonged residence in the apatite fission track partial annealing zone.

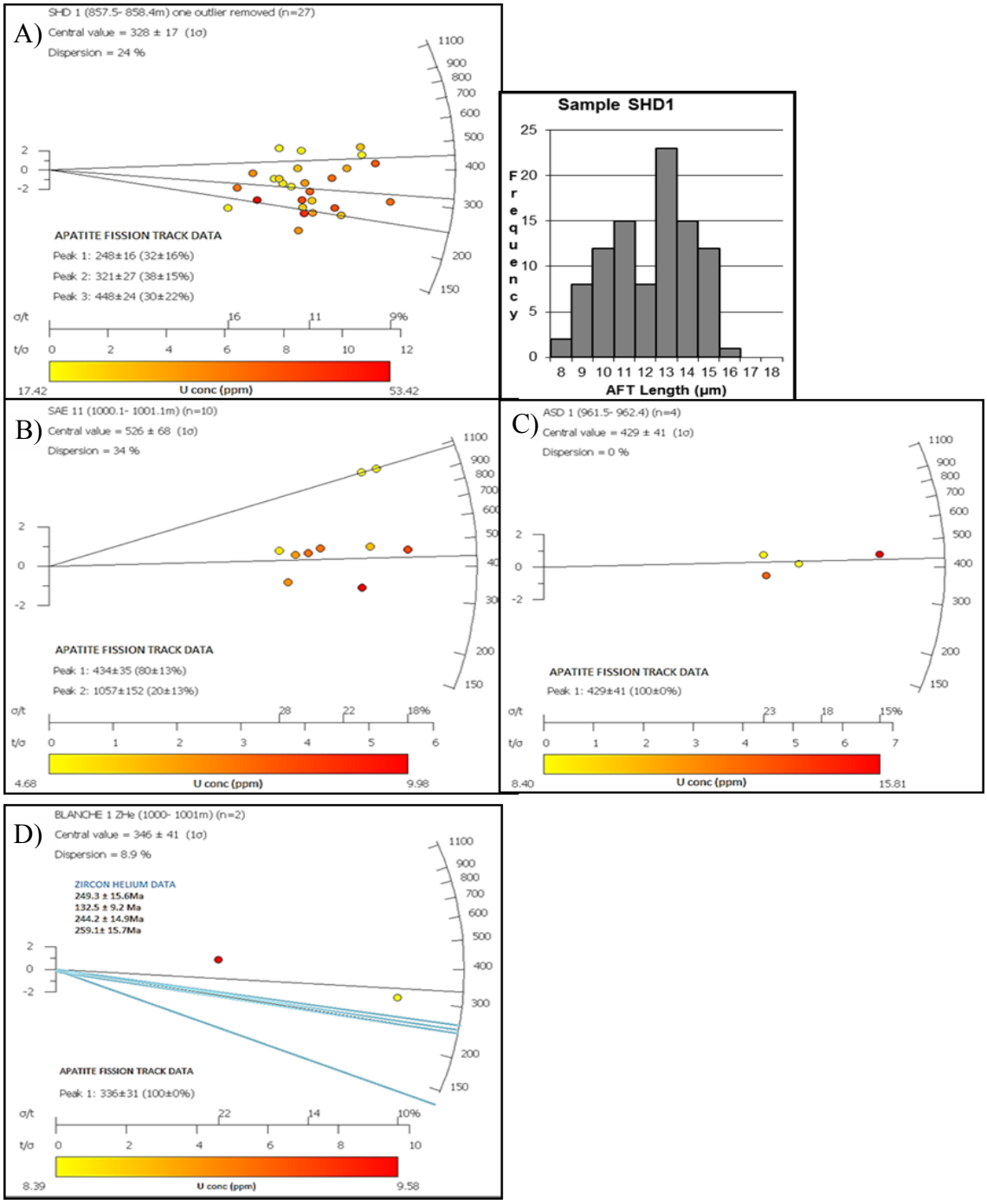

Figure 5:

Radial plots of single grain apatite fission track ages for deep samples (>800m), in order are a) SHD1, b) SAE 11, c) ASD 1 and d) BLANCHE 1. AFT peak ages are represented by black lines and blue lines show ZHe grain ages the age for each point on the diagram is obtained by projecting a line from the origin onto the right curved axis in Ma. The central age for the sample is given at the top of the figure. A key feature of the radial plot is that all points have the same error bar indicated by the axis about the origin on the left showing ± 2σ. The closer an individual data point is to the age axis (right side), the more precise the measurement is, as seen by the horizontal precision axis directly below the plot (Boone *et al.* 2013). The colour assigned to each individual point indicates the uranium concentration in ppm of that particular grain, which corresponds to the colour scheme illustrated at the bottom of the figure. The units for the uranium scale are ppm. This plot was constructed using Radial plotter (Vermeesch *et al*., 2009).

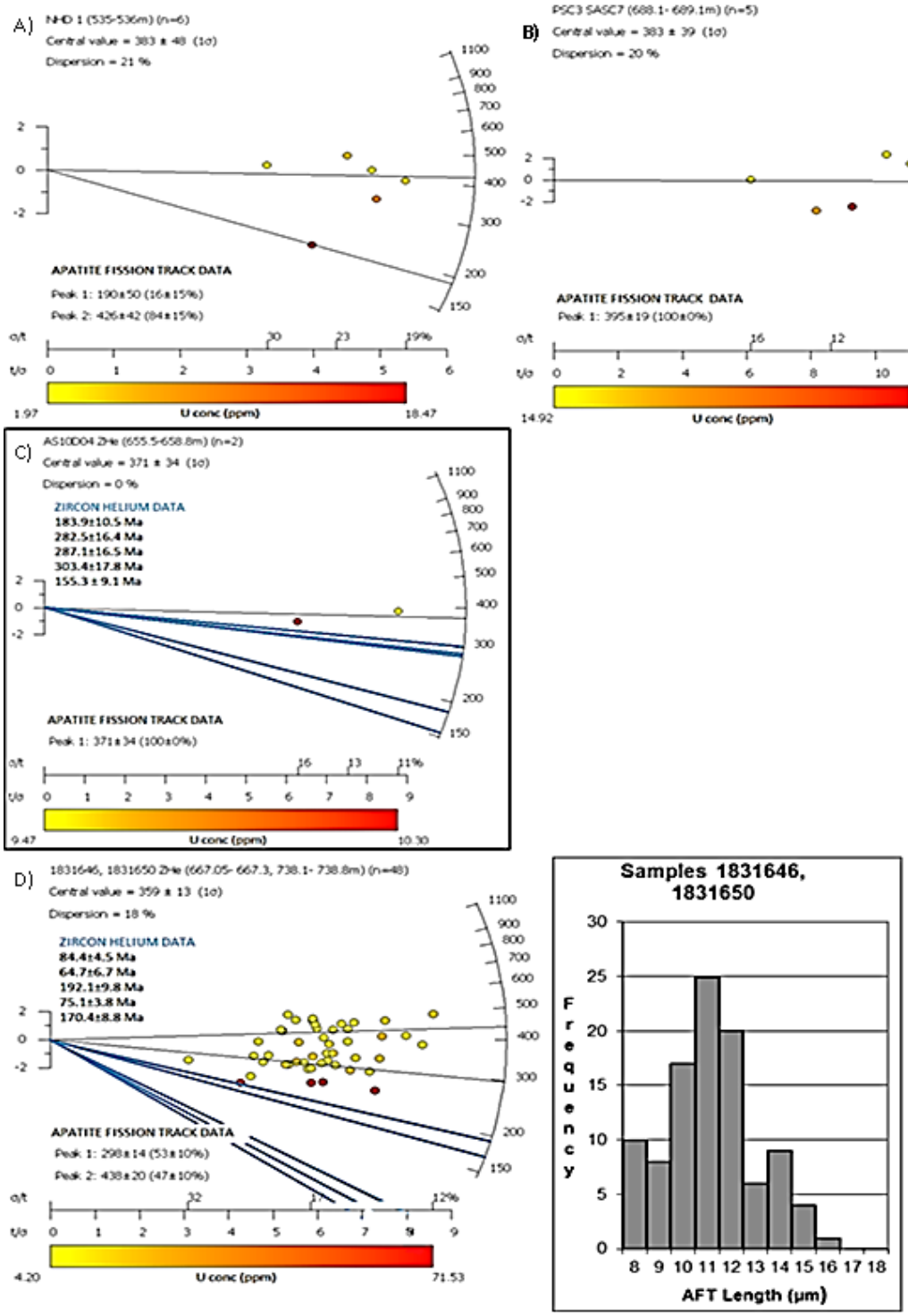

Figure 6

Intermediate samples Radial plots of single grain apatite fission track ages for intermediate depths (500-800m) in order are a) NHD1, b) PSC3SASC7, c)AS10D04, and d)1831646 1831650 pooled. AFT age peaks are shown in black lines and ZHe ages are shown by green lines. The age for each point on the diagram is obtained by projecting a line from the origin onto the right curved axis in Ma. The central age for the sample is given at the top of the figure. A key feature of the radial plot is that all points have the same error bar indicated by the axis about the origin on the left showing ± 2σ. The closer an individual data point is to the age axis (right side), the more precise the measurement is, as seen by the horizontal precision axis directly below the plot (Boone et al., 2013). The colour assigned to each individual point indicates the uranium concentration in ppm of that particular grain, which corresponds to the colour scheme illustrated at the bottom of the figure. The units for the uranium scale are ppm. This plot was constructed using Radial plotter (Vermeesch et al., 2009).

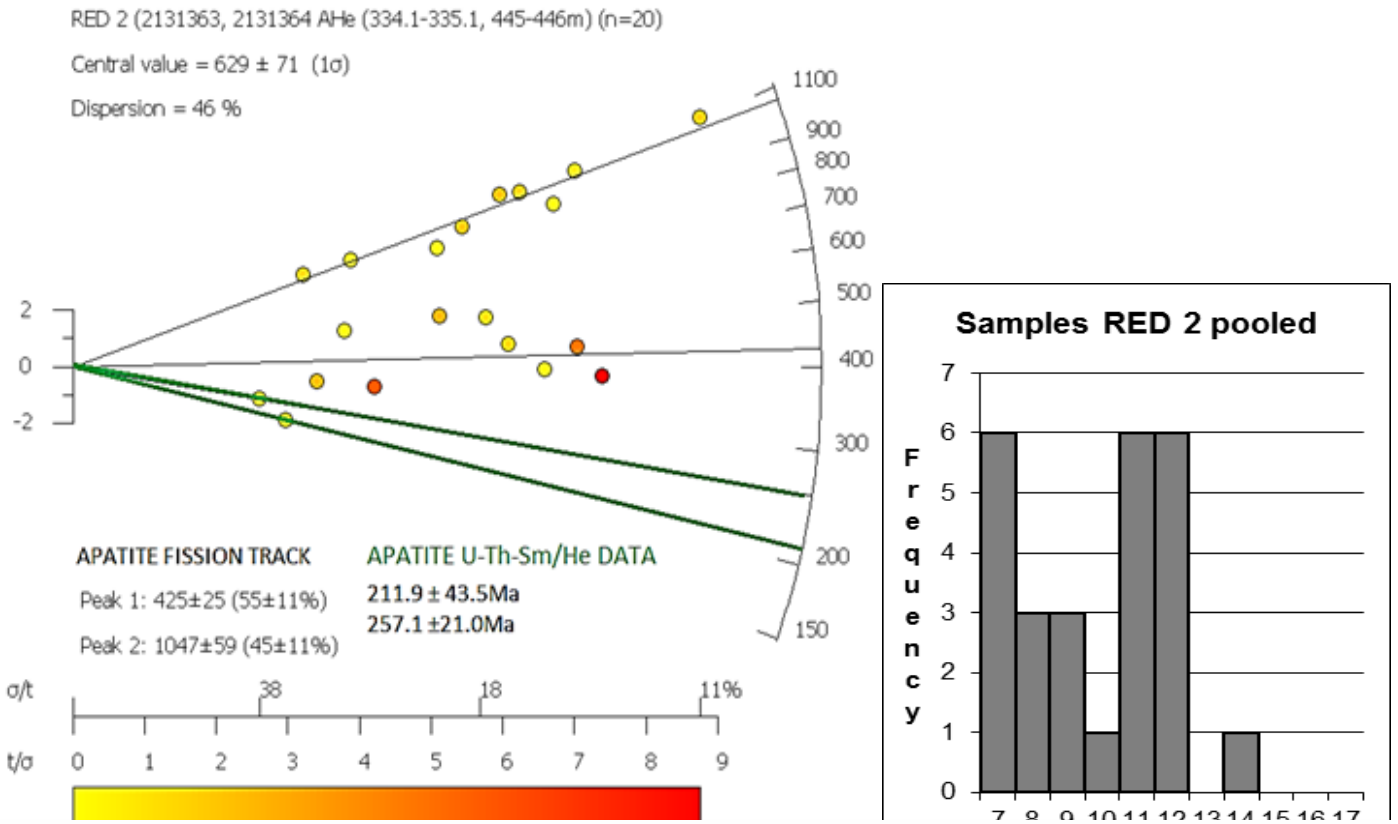

Figure 7:

Radial plots of single grain apatite fission track ages for the shallowest samples taken. AFT peaks ages are in black and green lines represent AHe peak ages. The age for each point on the diagram is obtained by projecting a line from the origin onto the right curved axis in Ma. The central age for the sample is given at the top of the figure. A key feature of the radial plot is that all points have the same error bar indicated by the axis about the origin on the left showing ± 2σ. The closer an individual data point is to the age axis (right side), the more precise the measurement is, as seen by the horizontal precision axis directly below the plot. The colour assigned to each individual point indicates the uranium concentration in ppm of that particular grain, which corresponds to the colour scheme illustrated at the bottom of the figure. The units for the uranium scale are ppm. This plot was constructed using Radial plotter (Vermeesch *et al.*, 2009).

DISCUSSION

Geographic location within the study area shows no plausible relationship with obtained AFT age peaks. Statistically reliable differences between samples can only be observed when they are grouped according to depth of drill core section samples were taken. Three groups were distinguished, consisting of samples taken from shallower than 500 metres, between 500-800 metres depth, and those deeper than 800 metres.

Samples taken from drill core RED 2 make comparison of individual radial plots based on the shallow group (figure 8a), samples NHD1, PAS 7 SASC3, AS10D04, 1831646 and 1831650 define samples taken at intermediate depths (figure 8b), and the deep group consists of samples SHD1, SAE11, BLANCHE 1, and ASD1 (figure 8c).

For the samples from the `shallow` group, 20 apatites were pooled and a central AFT age of 629 ± 71Ma was calculated as shown in figure 8(a). Given the rather large (46%) dispersion in single grain data, the AFT age population was decomposed into two peaks using the automatic mixer algorithm in Radial plotter (Vermeesch *et al.,* 2009). The oldest peak (comprising 45% of single grain ages) was constrained to the Mesoproterozoic (1047 ± 59 Ma), the youngest (based on 55% of the data) returned a 425 ± 25 Ma (Silurian) AFT age. Apatite (U-Th-Sm)/ He analysis of two apatite grains from sample 2131364 returned two age peaks, that are both significantly younger than corresponding AFT data: 257.1 ± 21 Ma (early Triassic) and 211.9 ± 43.5Ma (late Triassic). The combined dataset suggests that three low-temperature thermal events are preserved in the shallow upper crust at the RED 2 drilled location within the Stuart Shelf. Given that none of these events are recorded by multiple thermochronometric clocks and insufficient fission track length data could be obtained for this sample to perform thermal history modelling, more data is required to comment on the associated cooling rates with each thermal event.

The large scatter in AHe data furthermore indicates that the samples may have been affected by partial He loss and that the youngest thermal event is therefore potentially meaningless or at least not well constrained.

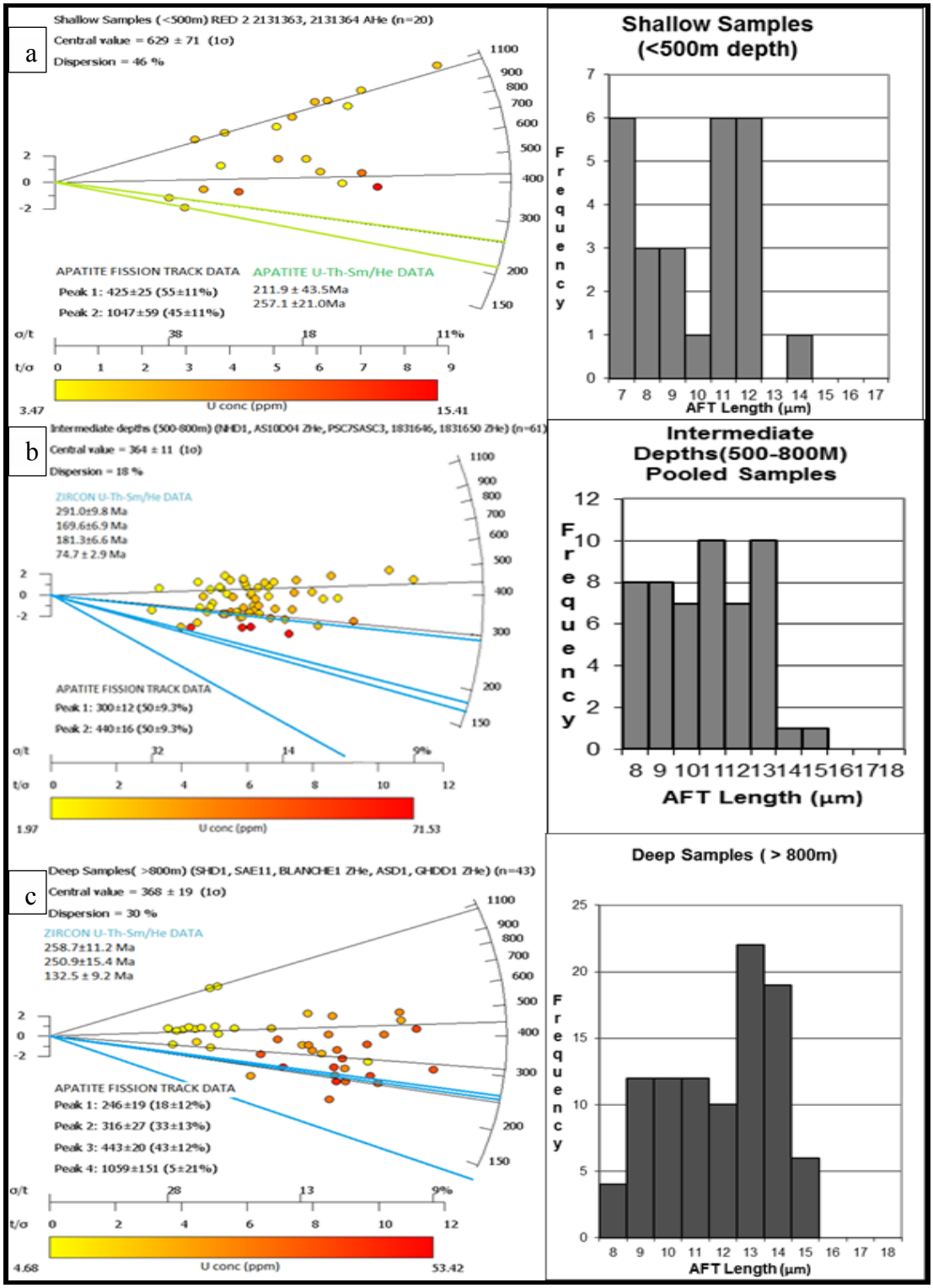

Figure 8: Radial plots of single grain apatite fission track ages for samples pooled by depth and corresponding length distribution histograms for pooled sets. A) shallow samples (<500m) B) shows intermediate samples (500-800m) and C) shows pooled data for samples below 800mThe age for each point on the diagram is obtained by projecting a line from the origin onto the right curved axis in Ma. The central age for the sample is given at the top of the figure. A key feature of the radial plot is that all points have the same error bar indicated by the axis about the origin on the left showing ± 2σ. The closer an individual data point is to the age axis (right side), the more precise the measurement is, as seen by the horizontal precision axis directly below the plot (Boone *et al.*, 2013). The colour assigned to each individual point indicates the uranium concentration in ppm of that particular grain, which corresponds to the colour scheme illustrated at the bottom of the figure. The units for the uranium scale are ppm. This plot was constructed using Radial plotter (Vermeesch *et al.*, 2009).

Pooled AFT age data for samples between 500-800 metres depth are shown in figure 8(b). A total of 61 apatites were analysed showing a central AFT age of 364 ± 11 Ma which was decomposed into two well-defined age peaks of late Silurian-early Devonian age (440 ± 16 Ma) and late Carboniferous-early Permian (300 ± 12 Ma) age. The peak discrimination process is largely supported by differences in single grain Uranium concentrations between both age clusters. This indicates that grains that underwent less radiation damage preserve the oldest AFT cooling ages. Pooled zircon (U-Th-Sm)/He data for those samples shows a large scatter (between ~300 and 70 Ma). The oldest ZHe data confirms the presence of a late Carboniferous- early Permian cooling event (291.0 ± 9.8 Ma). The other ZHe data are interpreted to be affected by Helium loss at varying degrees. Therefore it can be suggested that only two reliable thermal events can be distinguished during the late Silurian – early Devonian and late Carboniferous-early Permian. These cooling ages roughly correspond with the youngest thermal events (Ordovician) identified for the Red 2 shallow samples (discussed above), however, Mesoproterozoic ages, seen in the shallow data are not preserved at these depths.

The pooled data of samples from a depth greater than 800 metres, shown in figure 8(C), allows four AFT peak ages. Three of those are well defined to a late Silurian-early Devonian peak (443 ± 20 Ma), a late Carboniferous-early Permian peak (316 ± 27 Ma) and a late Permian- early Triassic peak (246 ± 19 Ma). Two additional apatites constrain a poorly defined Mesoproterozoic (~ 1059 ± 151 Ma) AFT age peak. Two zircon (U-Th-Sm)/ He peaks of late Permian -early Triassic ages (250.9 ± 15.4 Ma, 258.7 ± 11.2 Ma) support the late Permian-early Triassic peak (248 ± 17 Ma) observed in the AFT data. Younger ZHe data is likely affected by He loss as discussed above. Similarly as for the previous sample group, samples with higher Uranium concentrations seem to better preserve the older age peaks and vice versa. Discarding the two older AFT outliers, the pooled data for samples at the deepest sampled levels seem to correspond well with those at intermediate sampling depth,

indicating preservation of Silurian and Carboniferous thermal events. One additional Permian-Triassic thermal event was not well constrained at shallow and intermediate sample depths but was more pronounced at deeper sampling level.

When the data is collated (figure 9), four well defined thermal events can be distinguished, representing the preserved low-temperature thermal history record for the buried Stuart Shelf basement. These thermal events are constrained to the Mesoproterozoic (1050 ± 50 Ma), Silurian (439 ± 14 Ma), late Carboniferous-early Permian (304 ± 36 Ma) and late Permian-Triassic (245 ± 52 Ma). As discussed above, the preservation potential of these thermal events largely depend on the sample depth, with older events only preserved in the more shallow samples and vice versa.

The gaps is the regional low temperature exhumation of Australia (South Australia in particular) is seen in figure 10, which shows comparison between the central ages obtained by this study for the buried eastern Gawler Craton with all AFT central ages obtained by studies in the surrounding regions mentioned in this study

Tectonic interpretations

The Mesoproterozoic (1050 ± 50 Ma) thermal event are likely related to the final pulses of the Musgravian Orogeny (~1230 – 1150 Ma; Wade *et al.,* 2008). This age constraint also coincides with the end of the Pandurra Formation and emplacement/intrusion of the Beda Volcanic Suite (1070 Ma; Preiss *et al.,* 1987). However, conclusive evidence for tectono-thermal events in the Gawler Craton during this time are lacking, so this age peak may be just a localised event. In this regard, Keeling et al (2007) gives an age of~1100 Ma for hydrothermal alteration of dicktite to illite in the base of the Pandurra Formation. This alteration requires localised fluid flow at temperatures > 150 °C, above the apatite PAZ.

Excluding the Mesoproterozoic AFT data, the oldest exhumation pulse seen in the pooled plot (figure 9) is ~440 Ma. The large spread of single grain ages (~500 - 400 Ma) associated with this peak indicates mixing between the Delamerian Orogeny (514 – 490 Ma; Foden *et al.,* 2006), represented by the oldest AFT ages (480 Ma) with partial resetting of AFT ages by the first pulse of the Alice Springs Orogeny (ASO) (~450 Ma (Raimondo *et al.,*. 2014). Crustal thickening and exhumation throughout South Australia resulting from the ASO has been widely documented (Mitchell *et al.,* 1998; Gibson and Stüwe 2000).

Most samples (35 % of pooled AFT data) show evidence for a late Carboniferous- early Permian cooling pulse (304 ± 36 Ma) and although poorly constrained is supported by (U-Th-Sm)/ He peak within the standard error of the He peak age (figure 9). There are no other thermochronological constraints in the Stuart Shelf supporting a thermal event in the Carboniferous, however, several AFT studies in surrounding areas such as the Gawler Craton (Gleadow *et al.,* 2002, Boone *et al.,* 2013, Reddy Hons Thesis 2014); the Adelaide Fold Belt (Gibson and Stüwe *et al.,* 2000) and the Flinders Ranges (Weisheit *et al.,* 2014) also show evidence of Carboniferous exhumation linked to widespread crustal thickening throughout South Australia resulting from final stages of the ASO (Ballèvre *et al.,* 2000). The large smear seen in the single apatite grain ages seen in this study are thought to represent slow cooling through the Apatite Partial Annealing Zone (APAZ) due to the prolonged Phanerozoic exhumation of the Gawler Craton (Boone *et al.,* 2013; Reddy Hons 2014), which was enhanced by the far-field effects of the final pulse of the Alice Springs Orogeny (Sandiford and Hand 1998, Raimondo *et al.,* 2014).

A Triassic (246 ± 19 Ma) AFT age is preserved in samples from depths greater than 800m only. However shallow samples preserve a similar AHe age (234.5 ± 22.8 Ma) and similar ZHe ages (~240 Ma) are preserved in intermediate and deep samples without showing an preserved Jurassic AFT event. Several studies on the sedimentology of the Carboniferous- Permain glacial event indicate that

widespread post-Early Permain (post glacial) isostatic adjustment following glacial melting may have accelerated deposition in the Eromanga Basin to the north east of the study area and may have caused exhumation of the Stuart Shelf platform through the Apatite Partial Annealing Zone APAZ (Kuang et al., 1985).

Glacial erosional surfaces are seen over the present day Stuart Shelf Sequence (Preiss *et al.* 1987). Weisheit et al (2014) accounts for an event of localised Triassic- Jurassic hydrothermal resetting resulting in an AFT peak observed for the study conducted in the northern Flinders Ranges. Although it was previously thought to represent an event localised to the northern Flinders Ranges (Weisheit *et al.,* 2014) thermal reheating during the Mesozoic has been seen in regional studies as well (Gleadow, Kohn *et al.,* 2002; Boone *et al.,* 2013 etc.). There is no clear evidence supporting either post-glacial sedimentary burial or increased geothermal gradients to explain the reheating event, however the data from this study suggests that the perceived localised Triassic -Jurassic hydrothermal overprinting must have been regional, not only affecting the northern Flinders Ranges but areas of the Stuart Shelf also.

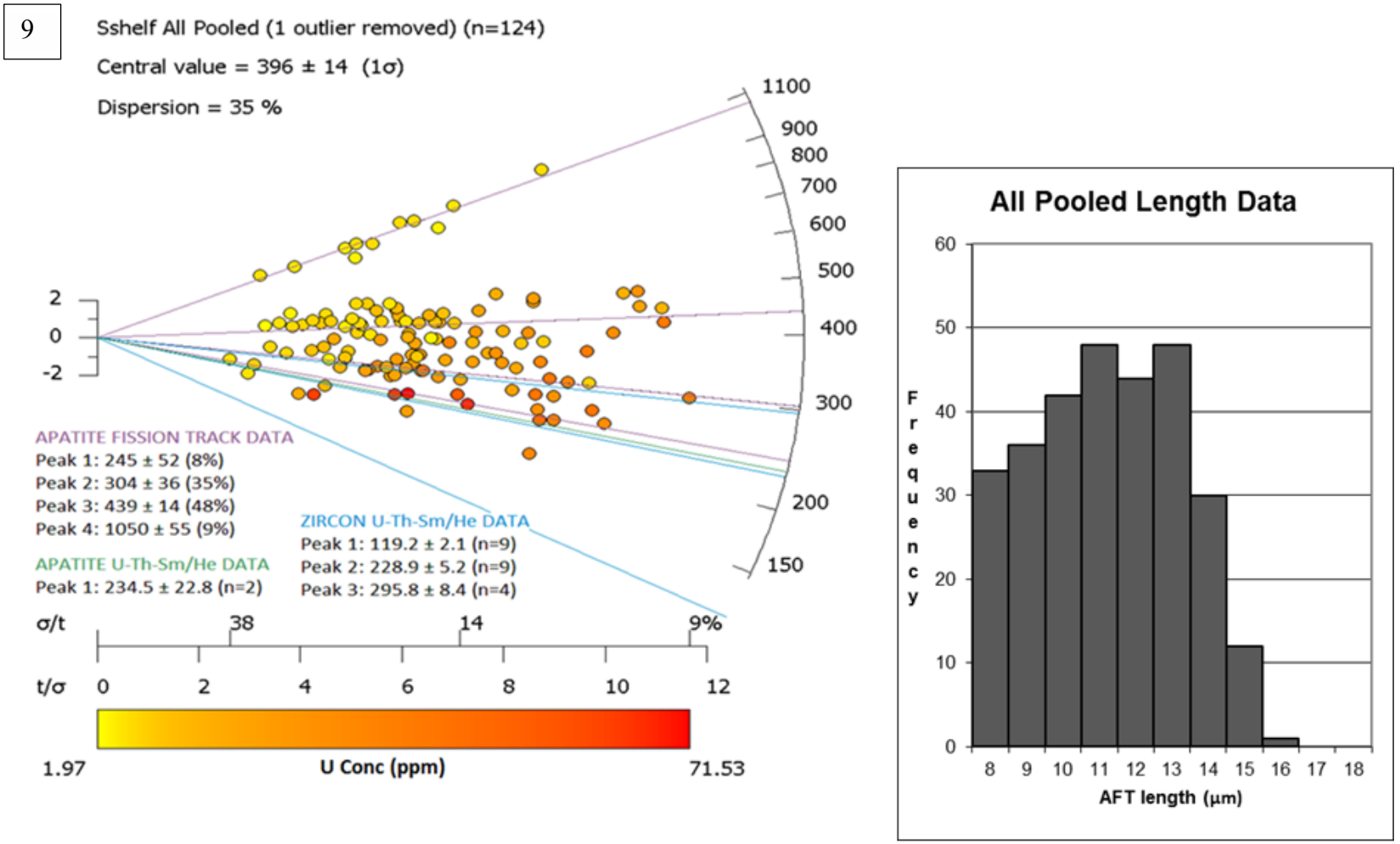

Figure 9 :Radial plots of single grain apatite fission track ages for all samples. AFT peaks are in purple, AHe peaks are in green and ZHe peaks are in blue. The age for each point on the diagram is obtained by projecting a line from the origin onto the right curved axis in Ma. The central age for the sample is given at the top of the

figure. A key feature of the radial plot is that all points have the same error bar indicated by the axis about the origin on the left showing ± 2σ. The closer an individual data point is to the age axis (right side), the more precise the measurement is, as seen by the horizontal precision axis directly below the plot (Boone *et al.,* . 2013). The colour assigned to each individual point indicates the uranium concentration in ppm of that particular grain, which corresponds to the colour scheme illustrated at the bottom of the figure. The units for the uranium scale are in parts per million (ppm). This plot was constructed using Radial plotter (Vermeesch *et al.,* 2009). The histogram shows the length distribution of measured confined tracks from all samples.

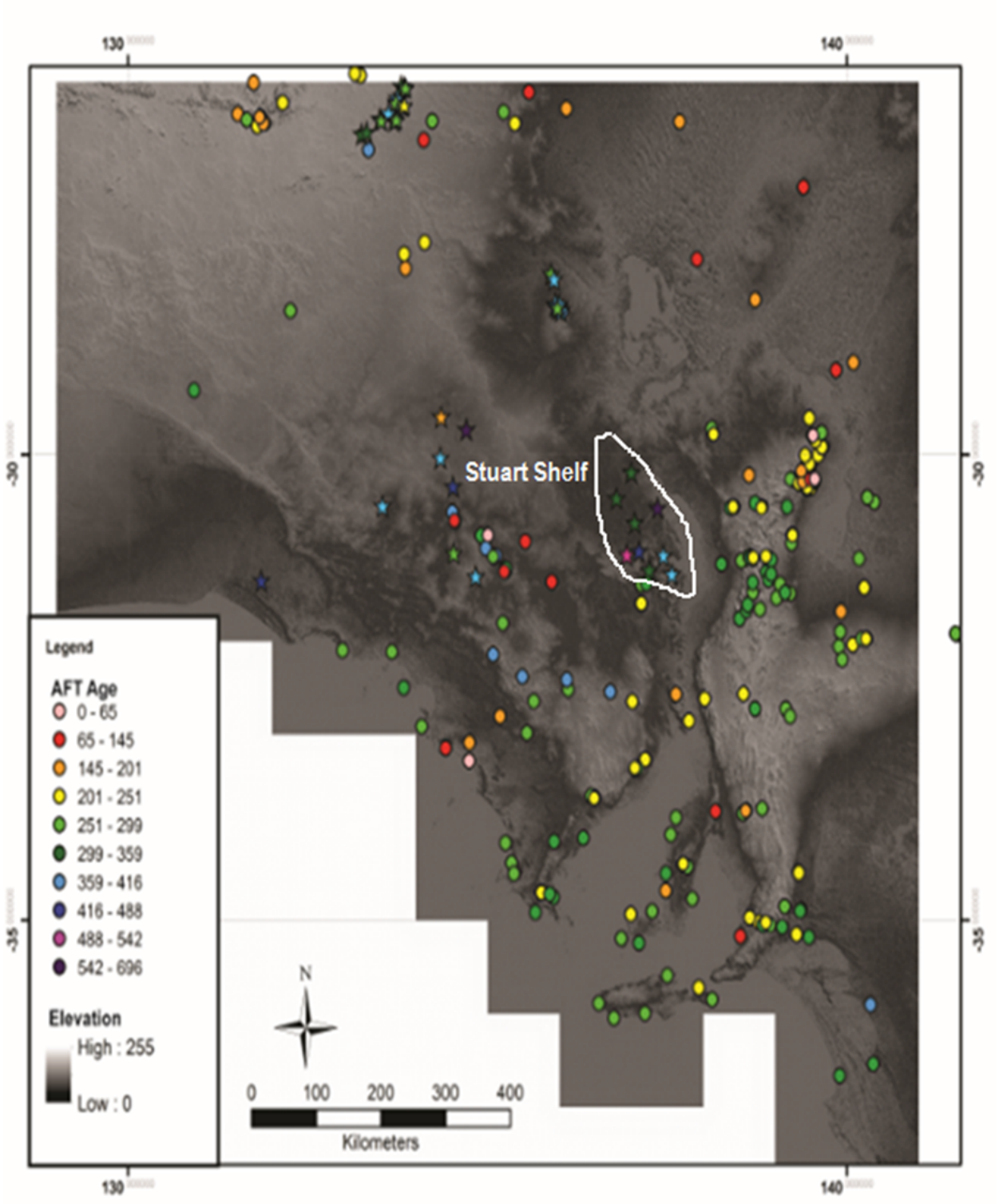

Figure 10: A TMI image indicating the gap is the regional low temperature exhumation of Australia (South Australia in particular) is seen in figure 10, which shows comparison between the central ages obtained by this study for the buried eastern Gawler Craton with all AFT central ages obtained by studies in the surrounding regions mentioned in this study.

CONCLUSIONS

Multi-method thermochronology applied to the eastern Gawler Craton margin concealed by the Stuart Shelf cover (Olympic Dam Domain, South Australia), identifies multiple thermal events, as presented above. The aim of this study was to identify whether the study area had underwent a similar low temperature thermal evolution as identified by studies carried out in the surrounding regions. Modelled data from Apatite Fission Track (AFT) analysis identified four time periods where the Gawler Craton basement below the Stuart Shelf experienced cooling into AFT closure temperatures (~60- 120 °C); at 1050 ± 55 Ma (Mesoproterozoic), 439 ± 14 Ma (late Ordovician-Silurian), 304 ± 36 Ma (mid-Carboniferous - mid Permian) and at 245 ± 52 Ma (late Permian - early Jurassic). The Mesoproterozoic AFT data appear to be oldest reported for South Australia, preserved in the buried basement of the Stuart Shelf. In neighbouring regions such as the Flinders ranges, this event has been completely reset by younger, Phanerozoic thermotectonic events, which were documented for the Stuart Shelf basement as well. The Carboniferous and Jurassic peaks are supported by zircon (ZHe) and apatite (AHe) (U-Th-Sm)/ He results. The Ordovician peak is interpreted as the result of the final pulses of the Delamerian Orogeny partially mixed with the first pulses of the Alice Springs Orogeny. The Carboniferous-Permian event is linked with widespread exhumation likely due to the final pulses of the Alice Springs Orogeny (~300 Ma). The late Permian-early Jurassic event is comparable to events believed to stem from hydrothermal events or post-glacial burial.

This study concludes that despite being buried beneath the Stuart Shelf, the eastern Gawler Craton has a complex low temperature thermal evolution comparable to that seen in the surrounding regions. The Mesoproterozoic pulse compliments previous studies on hydrothermal mineral alteration in the study area. The younger peaks indicate that the eastern Gawler Craton has experienced the distal effects of the Delamerian Orogeny, the beginning and final phases of the Alice Springs Orogeny, and

infer that hydrothermal activity in the Jurassic reached further than the northern Flinders Ranges. This study demonstrates that the separation of Australia from Antarctica in the Cretaceous had no low temperature effect on the eastern Gawler Craton, unlike the Adelaide Fold Belt, and the Flinders Ranges.

ACKNOWLEDGMENTS

This thesis was made possible thanks to the financial support of Department of State Development, South Australia and the University of Adelaide. I would like to thank Dr. Stijn Glorie for the countless hours of supervision, Dr. Anthony Reid for the sample donations, Prof. Alan Collins for his supervision. I would also like to thank Dr Katie Howard for her supervision and training. I would also like to thank The John De Laeter Centre at Curtin University for collecting the He data, and Adelaide Microscopy for the use of the LA-ICP-MS.I would like to thank Kate Agostino for help and Olwyn Mackay for help editing. Lastly I would like to give a massive thanks to James William Hall and hope the results of this study help to reconstruct a better interpretation of the Phanerozoic topographic evolution of central South Australia.

REFERENCE LIST

ADIE, R. J. (1962). The geology of Antarctica. In *Antarctic Research: The Matthew Fontaine Maury Memorial Symposium*. American Geophysical Union. pp. 26-39

BOONE S. C. (2013). Apatite Fission Track Anomaly within the Archean-Proterozoic Gawler Craton: The Thermal Record of a Paleoaquifer System. Masters Thesis. University of Melbourne, (unpublished).

B. P. KOHN , A. J. W. GLEADOW , R. W. BROWN , K. GALLAGHER , P. B. O'SULLIVAN & D. A. FOSTER (2002) Shaping the Australian crust over the last 300 million years: Insights from fission track thermotectonic imaging and denudation studies of key terranes, Australian Journal of Earth Sciences: An International Geoscience Journal of the Geological Society of Australia, 49:4, 697-717.

BRAUN, J., BURBIDGE, D. R., GESTO, F. N., SANDIFORD, M., GLEADOW, A. J. W., KOHN, B. P., & CUMMINS, P. R. (2009). Constraints on the current rate of deformation and surface uplift of the Australian continent from a new seismic database and low-T thermochronological [i]data. *Australian Journal of Earth Sciences*, *56*(2),pp. 99-110.

CZARNOTA, K., ROBERTS, G.G., WHITE, N.J., FISHWICK, S., 2014. Spatial and temporal patterns of Australian dynamic topography from River Profile Modeling. Journal of Geophysical Research: Solid Earth 119, 1384-1424.

COMPSTON, W. I. L. L. I. A. M., & WILLIAMS, I. S. (1986). Impact ejecta horizon within late Precambrian shales, Adelaide Geosyncline, south Australia.*Science*, *233*(4760),pp 198-199.

CRANSWICK, E., & NETWORK, P. S. (2009). Mashers Fault and the seismicity anticipated to be stimulated by the proposed open pit mine at Olympic Dam. In *Earthquake engineering in Australia: proceedings of the conference held by the Australian Earthquake Engineering Society in Newcastle, NSW* pp. 11-13.

DE GRAVE, J., GLORIE, S., RYABININ, A., ZHIMULEV, F., BUSLOV, M.M., IZMER, A., ELBURG, M., VANHAECKE, F., VAN DEN HAUTE, P.,(2012). Late Palaeozoic and Meso-Cenozoic tectonic evolution of the southern Kyrgyz Tien Shan: Constraints from multi-method thermochronology in the Trans-Alai, Turkestan-Alai segment and the southeastern Ferghana Basin. Journal of Asian Earth Sciences 44, pp. 149-168.

DREXEL, J. F., & PREISS, W. V. (1995). The Geology of South Australia. Vol. 2. The Phanerozoic. South Australian Geological Survey. *Bulletin*, *54*.

DREXEL, J. F., PREISS, W. V., & PARKER, A. J. (Eds.). (1993). *The Geology of South Australia: The Precambrian* (Vol. 54). Mines and Energy, South Australia, Geological Survey of South Australia.

DYKSTERHUIS S. & MÜLLER R. D. (2008). Cause and evolution of intraplate orogeny in Australia. Geology 36,pp. 495-498

FARLEY K. A. 2002. (U-Th)/He Dating: Techniques, Calibrations, and Applications. Reviews in Mineralogy and Geochemistry 47, 819-844.

FERRACCIOLI, F., COREN, F., BOZZO, E., ZANOLLA, C., GANDOLFI, S., TABACCO, I., & FREZZOTTI, M. (2001). Rifted crust at the East Antarctic Craton margin: gravity and magnetic interpretation along a traverse across the Wilkes Subglacial Basin region. *Earth and Planetary Science Letters*, *192*(3),pp. 407-421.

FOSTER D. A. & EHLERS K. (1998). 40Ar–39Ar thermochronology of the southern Gawler Craton, Australia: implications for Mesoproterozoic and Neoproterozoic tectonics of East Gondwana and Rodinia. Journal of Geophysical Research 103, 10 pp.177– 193.

FOSTER D. A., MURPHY J. M. & GLEADOW A. J. W. (1994). Middle tertiary hydrothermal activity and uplift of the northern flinders ranges, South Australia: Insights from apatite fission-track thermochronology. *Australian Journal of Earth Sciences* 41,pp. 11-17.

FRASER, G., REID, A., & STERN, R. (2012). Timing of deformation and exhumation across the Karari Shear Zone, north-western Gawler Craton, South Australia.*Australian Journal of Earth Sciences*, *59*(4), pp.547-570.

GLEADOW, A. J. W., KOHN, B. P., BROWN, R. W., O'SULLIVAN, P. B., & RAZA, A. (2002). Fission track thermotectonic imaging of the Australian continent. *Tectonophysics*, *349*(1),pp. 5-21.

GLEADOW, A. J., BELTON, D. X., KOHN, B. P., & BROWN, R. W. (2002). Fission track dating of phosphate minerals and the thermochronology of apatite.*Reviews in mineralogy and geochemistry*, *48*(1), pp. 579-630.

GOW, P. A., WALL, V. J., & VALENTA, R. K. (1993). The regional geophysical response of the Stuart Shelf, South Australia. *Exploration Geophysics*, *24*(3/4),pp. 513-520.

HALL, J (2014). Exhumation of the Peake and Denison Ranges; insights from low-temperature thermochronology. University of Adelaide. Honours Thesis (unpublished).

HAND, M., REID, A., & JAGODZINSKI, L. (2007). Tectonic framework and evolution of the Gawler Craton, southern Australia. *Economic Geology*, *102*(8), pp.1377-1395

JAGODZINSKI, E. The age of magmatic and hydrothermal zircon at Olympic Dam.

KUANG, K.S. (1985) History and style of Cooper-Eromanga Basin structures. *Exploration Geophysics,* 16(2/3) pp.245-249.

LE HERON, D. P. (2012). The Cryogenian record of glaciation and deglaciation in South Australia. *Sedimentary Geology*, *243*,pp. 57-69.

MACDONALD, J. D., HOLFORD, S. P., GREEN, P. F., DUDDY, I. R., KING, R. C., & BACKÉ, G. (2013). Detrital zircon data reveal the origin of Australia's largest delta system. *Journal of the Geological Society*, *170*(1),pp. 3-6.

MATTHEWS, C. (2009). Geothermal energy prospectivity of the Torrens Hinge Zone: evidence from new heat flow data. *Exploration Geophysics*, *40*(3), pp.288-300.

MCDOWELL F. W., MCINTOSH W. C. & FARLEY K. A. 2005. A precise 40Ar–39Ar reference age for the Durango apatite (U–Th)/He and fission-track dating standard. Chemical Geology 214, 249-263.

MCKAY, A. D., & MIEZITIS, Y. (2001). *Australia's uranium resources, geology and development of deposits*. AGSO-Geoscience Australia.

MITCHELL, M. M., KOHN, B. P., & FOSTER, D. A. (1998). Post-orogenic cooling history of eastern South Australia from apatite FT thermochronology. In*Advances in fission-track geochronology* pp. 207-224. Springer Netherlands.

MITCHELL, M. M., KOHN, B. P., O'SULLIVAN, P. B., HARTLEY, M. J., & FOSTER, D. A. (2002). Low-temperature thermochronology of the Mt Painter Province, South Australia. *Australian Journal of Earth Sciences*, *49*(3), pp. 551-563.

MOST, A. G. T. A. S., & CHALLENGES, I. (2010). GOMA (Gawler Craton–Officer Basin–Musgrave Province–Amadeus Basin) Seismic and MT Workshop 2010.

NEUMANN, N. L., & FRASER, G. L. (2007). *Geochronological synthesis and time-space plots for Proterozoic Australia*. Geoscience Australia.

NEUMANN, N., SANDIFORD, M., & FODEN, J. (2000). Regional geochemistry and continental heat flow: implications for the origin of the South Australian heat flow anomaly. *Earth and Planetary Science Letters*, *183*(1), pp.107-120.

Olympic Dam Expansion: Draft Environmental Impact Statement (2009). BHP Billiton, 2009.

PARKER, A.J., DALY, S.J., FLINT, D.J., FLINT, R.B., PREISS, W.V. and TEALE, G.S. (1993). Paleoproterozoic. In:Drexel, J.F., Preiss, W.V. and Parker, A.J. (Eds) The geology of South Australia; Volume 1,The Precambrian. - Geological Survey of South Australia. Geological Survey of SouthAustralia Bulletin 54, pp.50-105.

PAYNE, J. L., BAROVICH, K. M., & HAND, M. (2006). Provenance of metasedimentary rocks in the northern Gawler Craton, Australia: implications for Palaeoproterozoic reconstructions. *Precambrian Research*, *148*(3), pp. 275-291.

PEARCE, N. J.G ., PERKINS, W. T.,. AND WESTGATE, J. A. (1997), The Development of Laser Ablation ICP-MS and Calibration Strategies: Examples from the Analysis of Trace Elements in Volcanic Glass Shards and Sulfide Minerals. Geostandards Newsletter, 21: pp. 175–190.

PREISS, W. V., ALEXANDER, E. M., COWLEY, W. M., & SCHWARZ, M. P. (2002). Towards defining South Australia's geological provinces and sedimentary basins. MESA Journal, 27, pp. 39-52.

PREISS, W. V. (2000). The Adelaide Geosyncline of South Australia and its significance in Neoproterozoic continental reconstruction. *Precambrian Research*, *100*(1),pp.21-63.

PREISS, W. V., (1987) (Compiler). The Adelaide Geosyncline- late Proterozoic stratigraphy, sedimentation, palaeontology and tectonics. South Australia. Geolocical Survey. Bulletin,53.

RADKE F. 1973 Fission-Track dating. Progress Report. (unpubl.): Amdel Project.

REDDY, M (2014) Low Temperature thermochronologic insights into the exhumation of the northern Gawler Craton (South Australia) University of Adelaide. Honours Thesis (unpublished)

REINERS P. W., SPELL T. L., NICOLESCU S. & ZANETTI K. A. (2004). Zircon (U-Th)/He thermochronometry: He diffusion and comparisons with 40Ar/39Ar dating. Geochimica et Cosmochimica Acta 68, pp.1857-1887.

REYNOLDS S. D., MILDREN S. D., HILLIS R. R. & MEYER J. J. (2006). Constraining stress magnitudes using petroleum exploration data in the Cooper–Eromanga Basins, Australia. Tectonophysics 415, pp.123–140.

ROSE, C. V., MALOOF, A. C., SCHOENE, B., EWING, R. C., LINNEMANN, U., HOFMANN, M., & COTTLE, J. M. (2013). The end-Cryogenian glaciation of South Australia. *Geoscience Canada*, *40*(4), pp. 256-293.

SKIRROW, R. G., BASTRAKOV, E. N., BAROVICH, K., FRASER, G. L., CREASER, R. A., FANNING, C. M., ... & DAVIDSON, G. J. (2007). Timing of iron oxide Cu-Au-(U) hydrothermal activity and Nd isotope constraints on metal sources in the Gawler craton, south Australia. *Economic Geology*, *102*(8), pp. 1441-1470.

TEASDALE, J., PRYER, L., ETHERIDGE, M., ROMINE, K., STUART-SMITH, P., COWAN, P., ... & HENLEY, P. (2001). Officer Basin SEEBASE Project.*Primary Industries, South Australia*.accessed at http://www.pir.sa.gov.au/__data/assets/pdf_file/0010/35794/srk_officer_report.pdf

TINGATE, P.R., DUDDY, I.R., (2002). The thermal history of the eastern Officer Basin (South Australia): evidence from apatite fission track analysis and organic maturity data. Tectonophysics 349, pp. 251-275.

TWIDALE, C. R. (2000). Early Mesozoic (? Triassic) landscapes in Australia: evidence, argument, and implications. *THE JOURNAL OF GEOLOGY*, *108*(5), pp.537-552.

VERMEESCH P. 2009. RadialPlotter: a Java application for fission track, luminescence and other radial plots. Radiation Measurements 44, 409-410.

WAGNER, G. A., & HAUTE, P. (1992). *Fission-track dating* (Vol. 6). Springer Science & Business Media

WATERHOUSE, J. D., PUHALOVIC, A., & GARNHAM, R. (2002). Hydrogeology of the Stuart shelf in South Australia and impacts of the Olympic dam mine.

WILLIAMS, G. E. (1998). Late Neoproterozoic periglacial aeolian sand sheet, Stuart Shelf, South Australia*. *Australian Journal of Earth Sciences*, *45*(5),pp. 733-741.

APPENDIX A: EXTENDED METHODOLOGY

Samples

Fourteen granitoid and volcanic rock samples were selected from drill cores taken along a roughly north south transect along the Stuart Shelf. Samples were obtained following a NS transect, taken from granitic basement of the eastern Gawler Craton below the Pandurra (Adelaidean) unconformity of the Stuart Shelf platform. Samples BRD 1, Blanche 1, SAE 6, and two samples from drill hole MGD 45,; 1831650, 1831646, were all taken from the Mesoproterozoic Hiltaba Suite Granite; samples PSC 7 SASC 3, SAE 11, GHDD 1, and two samples from DH RED 2, 2131363 and 2131364 were taken from the Mesoproterozoic Gawler Range Volcanics. Sample SHD 1 was taken from the Gneissic, Hutchinson group of Paleoproterozoic age, sample AS10D04 was taken from the Paleoproterozoic Donnington Granite Suite, sample NHD 1 was taken from un-named gneissic granite with of Mesoproterozoic age and sample ASD 1 was taken from a fine grained gabbro of unknown age. Samples were taken from sections selected for homogeneity, free from indication of hydrothermal alteration, quartz veining, and mineral inclusions.

Crushing

Apart from samples received as separate's, the remainder of the whole samples underwent crushing. The selected samples were crushed down from quarter core sections to a grain size suitable for separation and mounting. Pieces of sample were crushed using a large Jaw Crusher and then milled using a ring mill. Samples were then mill grinded multiple times in a gradient that started from a high (approx. 5mm gap between the plates) to a low (less than 1 mm between the mill plates.) Milled sample

was then sieved using a Sieve Shaker to separate the grains into three sizes >425µm, 425-79µm, and <79µm. The Ring Mill and Sieve Shaker process was repeated on the >425µm sized grains to increase the amount of grains of size 425-79µm which are the optimal size for this study and all of which underwent the process of mineral separation.

Mineral Separation

The resulting refined 425µm-79µm sample portions, were panned in water to remove a majority of the lighter minerals and to keep the denser mineral grains (much the same way one pans for gold). This also decreases the volume of minerals passed through the Franz Isodynamic Seperator (Franz for short) and Heavy Liquid Seperation. Resulting panned light minerals were dried in a low temperature oven (<70°C) and when dry were bagged filed away for future use if necessary. The remaining minerals were placed in a fume cupboard to aid in drying. Once dried, a magnet was passed over the sample to remove all highly magnetic minerals. These resulting minerals were stored for possible later use. The remaining minerals were processed through the Franz to remove any residual magnetic minerals. The first cycle of processing through the Franz was on 0.5 Amperes, after which a second run of the mineral grains unmoved by the Franz were processed again at 1.4 Amperes. The magnetic minerals from both runs were combined and retained for further potential use. The minerals which passed through the Franz both runs were separated based on density, using the heavy liquid Methylene Iodide (which had to be first diluted by 0.6% to ensure the recovery of apatite grains. The content of the bottle previously used was 60mL, and this was diluted with 3.5mL of Acetone to give a dilution of 6-7% (as suggested by Dr Stijn Glorie.). The grains that sank to the bottom of the heavy liquid were collected and rinsed with acetone to remove all traces

of the heavy liquid. The grains that did not sink were also rinsed and retained for future use if needed.

Picking

The resulting apatite grains that sank to the bottom of the heavy liquid were picked using a needle under two Olympus SZ61 microscopes placed side by side. A clear dish was placed under the first microscope into which the resulting mineral grains were loosely placed, and the second dish under the other microscope contained standard glass slides placed on top of one another. The slide on the bottom had one or two small crosses placed on it to act as a guide for placement of individual suitable apatite grains within a raster of suitable size. Inclusion free apatite grains with euhedral to subhedral grain shape, were picked and placed on the double sided tape using the crosses below as a guide for the raster. Rasters of 12 x 12 grains at least were preferred, but not all sampled yielded such a quantity of preferable grains, in which case smaller rasters were used (from Hall Hons Thesis 2014)

Mounting, Grinding and Polishing

Mounting of the grains is required to ease the process of counting and to ensure the grains are not lost during the LA-ICP-MS sessions. Before mounting can occur, glass slides have to be placed in an array. The array is as follows: the glass slide with the apatite raster in the centre, at each end, one slide perpendicular to the end of the apatite slide, one more slide at each end on top of the slides, perpendicular with the apatite

slide and about 1 cm onto the end of the apatite slide. Once the resin is placed on the apatite slide, a final slide is laid on top of the array directly on top of the apatite slide, this ensures there is one slide length between these two slides. The grains were mounted in a mixture of epoxy Cure resin (20-8130-032) and epoxyCure hardener (20-8132-008) with a ratio of 5 : 1. 20 minutes of stirring the mixture was required to ensure it was mixed enough for it to be considered homogenous throughout. Once the mixture is homogeneous, small drops of it were placed on top of the apatite grain raster sitting on the double sided tape. The drops were big enough to cover the entire raster and must exceed one glass slide in height so the final slide in the array comes into contact and sticks to the resin.

The resin was left to harden over a period of 3-4 days before the two attached slides are separated using a razor blade. The razor blade has to slide between the double sided tape and the slide which the tape is attached to. Once it has completely removed the tape from the slide, the tape can be peeled off the resin, leaving the grains exposed at the top of the resin with the other end of the resin attached to the final slide in the array.

1. Once the tape is removed, the sample needs to be ground down to expose internal grain sections. The steps for grinding and polishing are as follows: Round the edges of the glass slide using Zinc Lapping Discs
2. Apply water to Waterproof Silicon Carbide Paper before grinding off the top layer of resin by applying equal pressure to the sample and moving the sample in a figure of eight around the wet carbide paper. Repeat this step, stopping to check the progress under a microscope constantly, until top layer of resin, all remaining tape and the top of the grains are removed. Begin with #1200 paper before using #2400 for finer grinding when grinding is nearing completion.

3. Once the samples are ground down to an adequate level, they must be polished. A Struers DP-U4 Cloth Lap with 3 µm or 1 µm polishing cloths and the associated diamond suspension polishing lubricant were used to polish the samples.
4. Polishing was completed in five minute blocks until fully polished, first on the 3 µm cloth and later on the 1 µm cloth for finer polishing. While polishing, the samples were held horizontal and were constantly rotated to apply an even polish on the sample. (from Hall Hons thesis 2014)

Etching

Once the samples were polished, they were submerged and etched in 5 M HNO3 which was at 20 °C for 20 seconds. After the 20 seconds, they were dropped in a jug of water to dilute all remaining acid on the samples. Etching of Samples is required to enable fission tracks to be seen under the microscope by dissolving the surface of the grain, thus increasing the size of the fission tracks (from Hall Thesis 2014)

Counting and Measuring

Uranium is found in trace amounts within the crystal lattice in apatite and when U undergoes spontaneous fission, it damages the crystal lattice, leaving a 'fission track' (Figure 2). Each fission track is the remnant of a single fission event (Gleadow *et al*. 2002a). Above a 60 °C, these fission tracks can anneal and above 120 °C, completely repair the crystal lattice. Therefore, below 60 °C (the closure temperature), the fission

tracks remain in the crystal lattice (Green *et al*. 1985). Between 60 – 120 °C (known as the partial annealing zone; PAZ), fission tracks are able to anneal but not completely repair the crystal lattice. The fission tracks anneal more (thus decreasing the length of the fission track) with more time spent within the PAZ. Shorter fission tracks indicate longer time spent within the PAZ therefore, indicating the rate of cooling. As fission tracks are only partially annealed within the PAZ, this is the temperature range which is revealed when the AFT age is concluded when etched fission tracks are counted and combined with the U concentration of the grain.

The degree of shortening is proportional to the cooling rate and hence length measurements can be used further constrain the thermal history of the samples. Tracks which are completely confined within the crystal lattice, horizontal and etched through the contact with another track (Figure 10; TINT) or cleavage (TINCLE) can be

measured to conclude the rate of cooling (Gleadow *et al*. 1986).

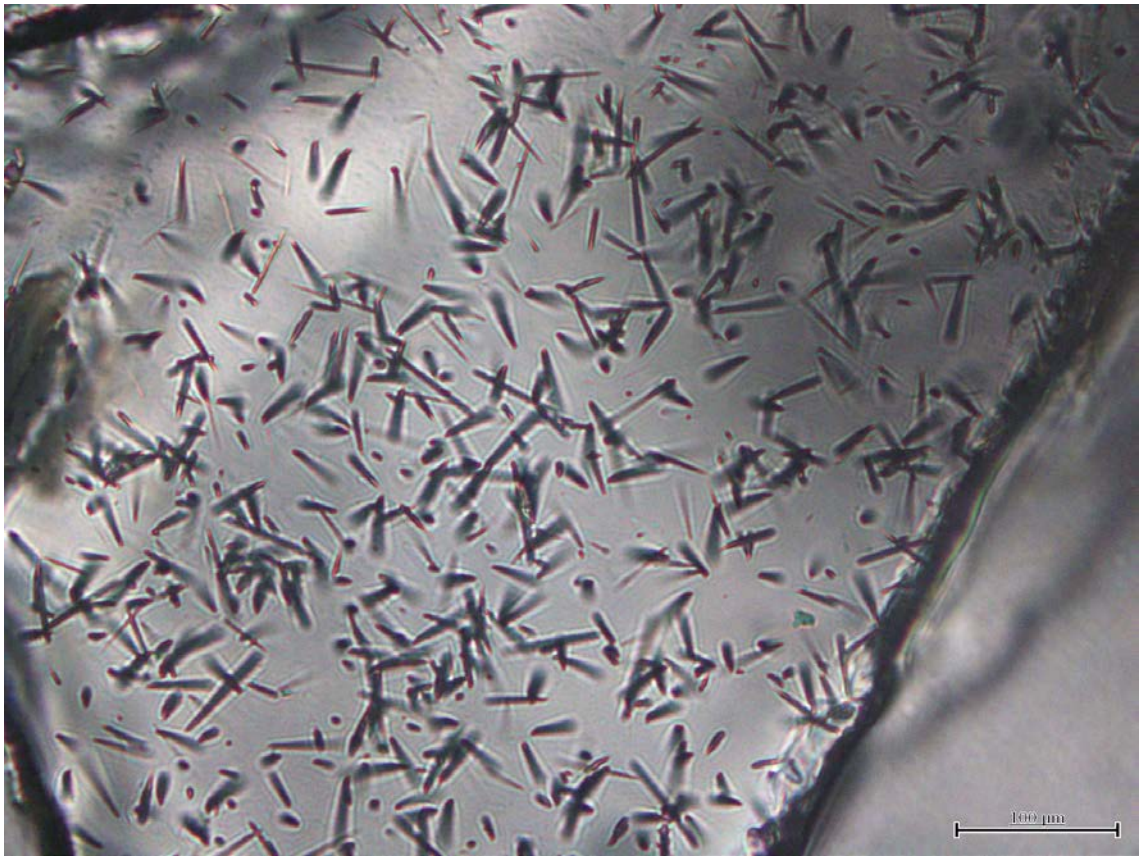

Figure Error! Main Document Only.**, an example of an etched apatite grain. The dark lines within the grain are the fission tracks. The photo is taken using transmitted light on an Olympus BX51 Microscope, with an Olympus DP21 camera and computer attachment, on 100x zoom from sample 1831650**

All counting and measuring was conducted on an Olympus BX51 Microscope, with an Olympus DP21 camera and computer attachment, on 100x zoom, using both transmitted and reflected light.

Counting was undertaken with the intention of counting 1000 fission tracks over 20-30 grains counted per sample.

Grains were selected for counting by passing a set of criteria:(from Hall Hons Thesis 2014)

1. Large enough grain size to count.
2. Random spread of fission tracks.
3. Reasonable amount of tracks, therefore, grains with too few or too many tracks were not counted.
4. Well-polished grains

Once a grain was selected for counting, the raster in the eye-piece was placed over the region of the grain to be counted and the dimensions of the counted area were documented. All the fission tracks were counted in the region and the final number was documented. A photograph was taken of the region for verification later. This process was repeated on all the grains possible until the goal number was reached.

The goal number for measuring was 100 confined tracks per sample, with a minimum of 20 confined tracks if only less than 20 confined tracks could be measured, these data was not used in further interpretations. All possible grains were checked for confined tracks and if the track could be verified to be horizontal and completely confined, its length was measured. The angle to the C-axis and 5 D_{par} (etch pit lengths) were also measured. Finally, the type of track-intersection (TINT or TINCLE) was noted. This was repeated on each sample until all the confined tracks had been measured, limited to 100 per sample.

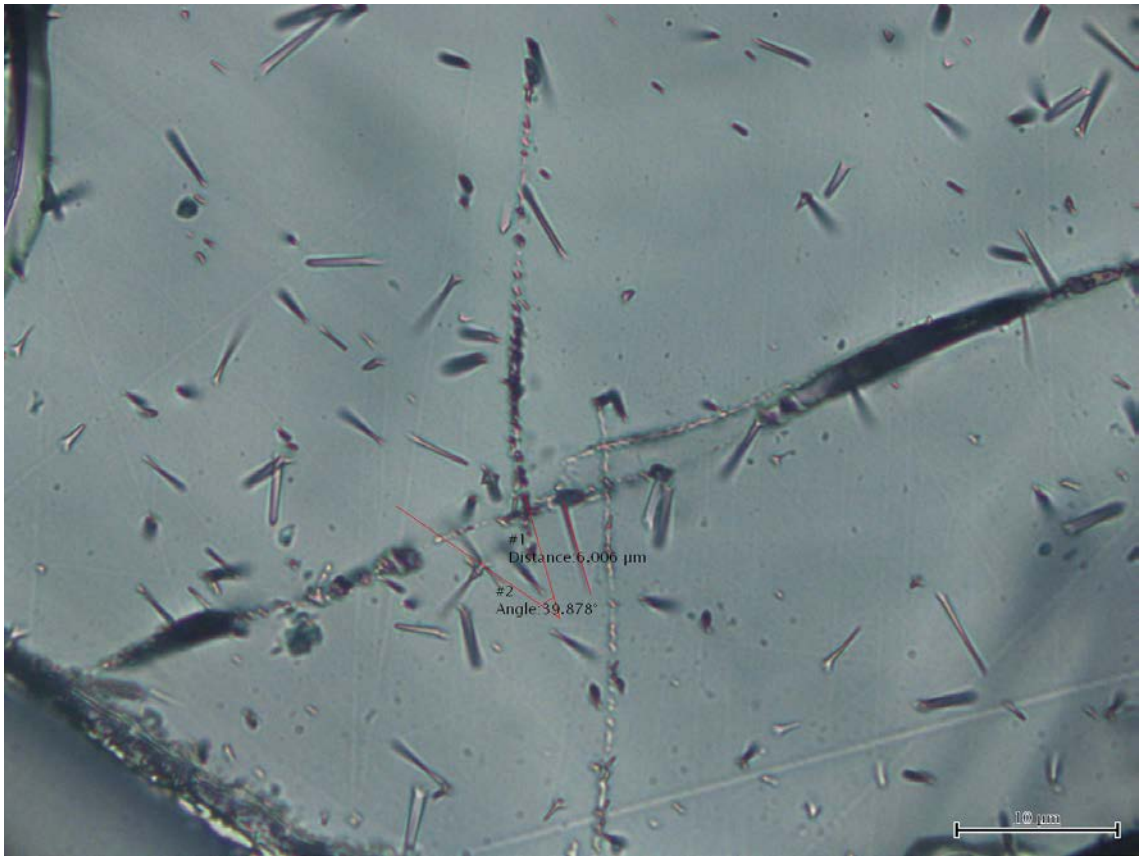

Figure Error! Main Document Only.**, an example of a confined track (a TINT in this example), as indicated by the red line covering the confined track. #1 distance indicates the length and location of the track, #2 indicates the angle of the track to the C-axis of the grain wile the last measurement indicates the length of an etch pit (D_{par}; measured in reflected light). The photo is taken using transmitted light on an Olympus BX51 Microscope, with an Olympus DP21 camera and computer attachment, on 100x zoom.**

LA-ICP-MS

The Laser-Ablation Inductively-Coupled-Plasma Mass-Spectrometer was used to conclude the concentrations of U^{238}, U^{235}, and Ca^{44}. This information was gathered by ablating the apatite crystals at the exact position (the actual spot size, which is listed in Table 1, used was often slightly smaller than the counted region. In this case, the spot

was placed in the centre of the counted area which is a valid approach if track counts appeared homogenous throughout the counted region.) which was counted as U and Ca concentrations can change over the grain (Hasebe *et al*. 2004) and allowing the Mass-Spectrometer to calculate the concentration . All information about the LA-ICP-MS used is identified in Table 4.

A total of 160 grains were sampled on the laser not including the two sets of standards, each sample was used in an exact sequence to allow for ease in the data reduction phase. One sequence consisted of 80 unknown measurements, therefore, the sequence was run twice to accommodate the 160.

The sequence is:

1. 3 Known glass standards (NIST 610, NIST 612 and NIST 614), each measured twice
2. 2 Apatite Durango standards
3. 8 unknowns from the samples (from Hall Hons thesis 2014)

(U-Th-Sm)/He Dating

(all details from James Hall's Honours Thesis 2014) Helium (^{4}He) diffusion through the radiogenic decay of Uranium and Thorium can be used to calculate the age at which rocks passed through a certain temperature as, above this closure temperature, ^{4}He can freely diffuse out of the mineral grain, however, below the closure temperature, the ^{4}He is trapped within the grain. Therefore, by determining the amount of ^{4}He to U and Th,

the age of the closure temperature (The closure temperature for apatite is 45 °C and around 170 °C for zircon) can be concluded (Farley 2002).

Two apatite separates and one zircon separate were picked using a picking needle under two Olympus SZ61 picking microscopes. Only the grains with the best grain shape, Over 70 µm in diameter and without inclusions or zonation were picked. These samples were sent to the John De Laeter Centre at Curtin University in Perth for (U-Th-Sm)/He Dating. For detailed methods of (U-Th)/He Dating at John De Laeter Centre, refer to Li *et al.* (2014).

Upon receiving the samples, grains which best suited the criteria for analysis were selected and measured for the calculation of an alpha correction factor (Farley *et al.* 1996).

Apatite:

He was extracted from the selected grains by loading the grains into platinum micro-crucibles and heated by a 1064 nm Nd-YAG laser. The U and Th concentration was concluded using isotope dilution. The Apatite was dissolved in 7 M HNO_3 over 12 hours and the resulting concentration of U and Th was recorded and calibrated against a standard using a Mass spectrometer.

Zircon:

The zircons were loaded into Niobium microvials and the He was extracted by heating the crystals to >1200 °C by a 1064 nm Nd-YAG laser. Isotope dilution inductively coupled mass spectrometry was used to determine the concentrations U and Th. The zircons were digested in 350 µl of HF for 40 hours, at 240 °C. Following this, 200 °C,

300 µl of HCl was used on each sample for 24 hours to dissolve any remaining fluoride salts. After the 24 hour period, the U and Th concentrations were measured with a mass spectrometer.